UNIVERSIDADE DA BEIRA INTERIOR
Engenharia

Single droplet ignition and combustion of jet-A1, hydroprocessed vegetable oil and their blends in a drop tube furnace

(Versão final após defesa)

Gonçalo de Sousa Pina Pernicha Pacheco

Dissertação para obtenção do Grau de Mestre em
Engenharia Aeronáutica
(ciclo de estudos integrado)

Orientador: Prof. Doutor André Resende Rodrigues da Silva
Co-orientador: Prof. Doutor Mário Manuel Gonçalves da Costa

Covilhã, fevereiro de 2020

Este trabalho foi realizado no âmbito da obtenção do grau de mestre de Gonçalo de Sousa Pina Pernicha Pacheco. Foi desenvolvido numa parceria entre a Universidade da Beira Interior e o Instituto Superior Técnico. O grau de mestre foi concedido pela Universidade da Beira Interior e o trabalho experimental decorreu no Instituto Superior Técnico.

Dedicatória

Em memória dos meus bisavós Manuel de Sousa e Ana de Sousa, que me ensinaram o que é o espírito de luta e perseverança. Obrigado por terem iniciado comigo este caminho e é com muita saudade que não têm a possibilidade de o verem terminado.

Acknowledgments

Firstly, I would like to express my sincere gratitude to my supervisors, Professor André Silva and especially Professor Mário Costa for providing me this opportunity and for all the support, knowledge and guidance. It was a challenge that helped me grow as an engineer and as a person.

I also sincerely thank Manuel Pratas for his technical support during the design of the experimental setup and for bringing always good mood to the laboratory. I would like to thank Pedro Rijo for his support during experimental tests and for the good debates about the experimental results, his help was indispensable during this work.

To my colleagues who I consider my friends, I want to thank them for their friendship, support and unique moments.

I would like to thank especially to Inês Ferrão who gave me all the love and suppord, and stayed by my side in every difficult time.

Lastly, I would like to express my gratitude to my family who always believed in me. Particularly to my parents and grandparents, for their unconditional support especially in the last difficult years. Without them, this journey would not be possible.

Resumo

O impacto ambiental e a dependência de combustíveis fósseis no setor aeronáutico promoveram a procura por combustíveis alternativos e ecológicos. Este é um dos principais desafios para este setor no futuro. Uma possível solução num futuro próximo pode ser a mistura de biocombustíveis com combustível de aviação, o que permitiria o uso de combustível mais ecológico e a redução de gases de efeito estufa e emissões sem alterações significativas nas frotas existentes das empresas, isto é, o desenvolvimento de um combustível "drop-in". Neste contexto, este trabalho examina as características de ignição e combustão de gotas isoladas de jet-A1 (JF), óleo vegetal hidroprocessado (NExBTL) e suas misturas num forno de queda livre (DTF). O objetivo deste trabalho é avaliar a influência da composição da mistura nas características do combustível. Gotas com diâmetros de 155 ± 5 µm, produzidas por um gerador comercial de gotas, foram injetadas no DTF, cuja temperatura da parede e concentração de oxigênio eram controladas. Os testes foram conduzidos para três temperaturas (900, 1000 e 1100 ºC). A ignição e a combustão das gotículas foram avaliadas através das imagens obtidas com uma câmara de alta velocidade acoplada a uma lente de alta ampliação e um algoritmo de deteção de limites. As imagens permitiram a observação dos fenómenos de queima e avaliar a evolução temporal do tamanho das gotas e das taxas de queima. Os resultados revelaram que as misturas de combustível seguem a lei D^2, exceto a mistura com 75% de JF para uma temperatura de 1100 ºC na parede do DTF. Isso ocorreu devido à ocorrência de *puffing* e micro-explosões, o que aumentou as taxas de queima. Observou-se ainda que as misturas com maior teor de JF apresentam chamas com maior intensidade luminosa e maiores taxas de queima.

Palavras-chave

Gota isolada, jet fuel, HVO, misturas, ignição, combustão, micro explosão, puffing

Abstract

The environmental impact and the dependence of fossil fuels in the aeronautical sector have promoted the demand for alternative and greener fuels. This is one of the main challenges for this sector in the near future. A possible solution in the near future might be the blending of biofuels with jet fuel, which would allow the use of greener fuels, and a reduction in the greenhouse gases and emissions without significant changes in the existing fleets of the companies, which means the development of a “drop in” fuel. In this context, this work examines the ignition and the combustion characteristics of single droplets of jet-A1 (JF), hydroprocessed vegetable oil (NExBTL) and their mixtures in a drop tube furnace (DTF). The objective of this work is to evaluate the influence of the fuel mixture composition on the fuel characteristics. Droplets with diameters of 155 ± 5 µm, produced by a commercial droplet generator, were injected into the DTF, whose wall temperature and oxygen concentration were controlled. Experiments were conducted for three temperatures (900, 1000 and 1100 ºC). The ignition and combustion of the droplets were evaluated through the images obtained with a high-speed camera coupled with a high magnification lens, and an edge detection algorithm. The images allowed for the observation of the burning phenomena, and data are reported for temporal evolution of droplet sizes and burning rates. The results revealed that the fuel mixtures followed the D^2 law, except the mixture with 75% JF for a DTF wall temperature of 1100 ºC. This was due to the occurrence of puffing and micro explosions, which enhanced the burning rates. In addition, it was observed that the mixtures with a higher content of JF present brighter flames, and higher burning rates.

Keywords

Single droplet, jet fuel, hydroprocessed vegetable oil, mixtures, ignition, combustion, micro explosion, puffing

Index

List of figures

List of tables

Nomenclature

Symbol	Designation	Units
CN	Cetane number	$-$
$c_{p,g}$	Specific heat at constant pressure	$[kJ/(kg.K)]$
D	Droplet diameter	$[mm]$
D_0	Initial droplet diameter	$[\mu m]$
f	Excitation frequency	$[kHz]$
FP	Flash point	$[^oC]$
FT	Fischer–Tropsch	$-$
G	Combustion group number	$-$
HHV	High heating value	$[MJ/Kg]$
I_w	Wobbe index	$-$
K	Burning rate	$[mm^2/s]$
LCV/LHV	Lower calorific value	$[MJ/Kg]$
M-E	Micro explosion	$-$
p	Pressure	$[Pa]$
Q	Volumetric flow rate	$[ml/min]$
Rd	Gas constant	$[kJ/(kg.K)]$
RF	Radiative forcing	$[W/m^2]$
Re_D	Droplet Reynolds number	$-$
Re	Reynolds number	$-$
S	Sutherland temperature	$[^oK]$
Sc	Schmidt number	$-$
SG	Specific Gravity	$-$
t	Time	$[s]$
T	Temperature	$[^oC]$

Greek symbols

μ	Dynamic viscosity	$[Pa.s]$
ρ	Density	$[kg/m^3]$

Subscripts

0	Initial
amb	Ambient
liq	Liquid
d	Droplet lifetime
g	Gas

List of acronyms

AJF	Alternative jet fuel
BtL	Biomass to liquid
DGS	Droplet generator system
DTF	Drop tube furnace
FAE	Fatty acid ester
FAEE	Fatty acid ethyl ester
FAME	Fatty acid methyl ester
Fps	Frames per second
FT	Fischer–Tropsch
GHG	Greenhouse gases
GTL	Gas to liquid
HEFA	Hydroprocessed esters and fatty acids
HVO	Hydroprocessed vegetable oil
HC	Hydrocarbons
HRJ	Hydroprocessed renewable jet fuel
IAS	Image acquisition system
ISA	International standard atmosphere
ICAO	International civil aviation organization
ROI	Region of interest
UHC	Unburnt hydrocarbons

Chapter 1

1. Introduction

In this chapter, the motivation of this study is presented in order to explain the importance of it. Thereafter, a literature review was elaborated to provide support, which includes the relevant studies for the present work.

1.1. Motivation

In just over 100 years, the aeronautical sector has had a notorious impact on the emergence of new markets. Consequently, new goods and services became essential in modern-day life. Commercial aviation has become a global business of around 22680 aircraft currently operating on a single fossil fuel. The sector is responsible for 2-3% of global carbon emission and it is expanding relatively fast with a predicted growth of 4.7% per year. This means that today's fleet will grow to almost 47680 aircraft by 2038 [1,2].

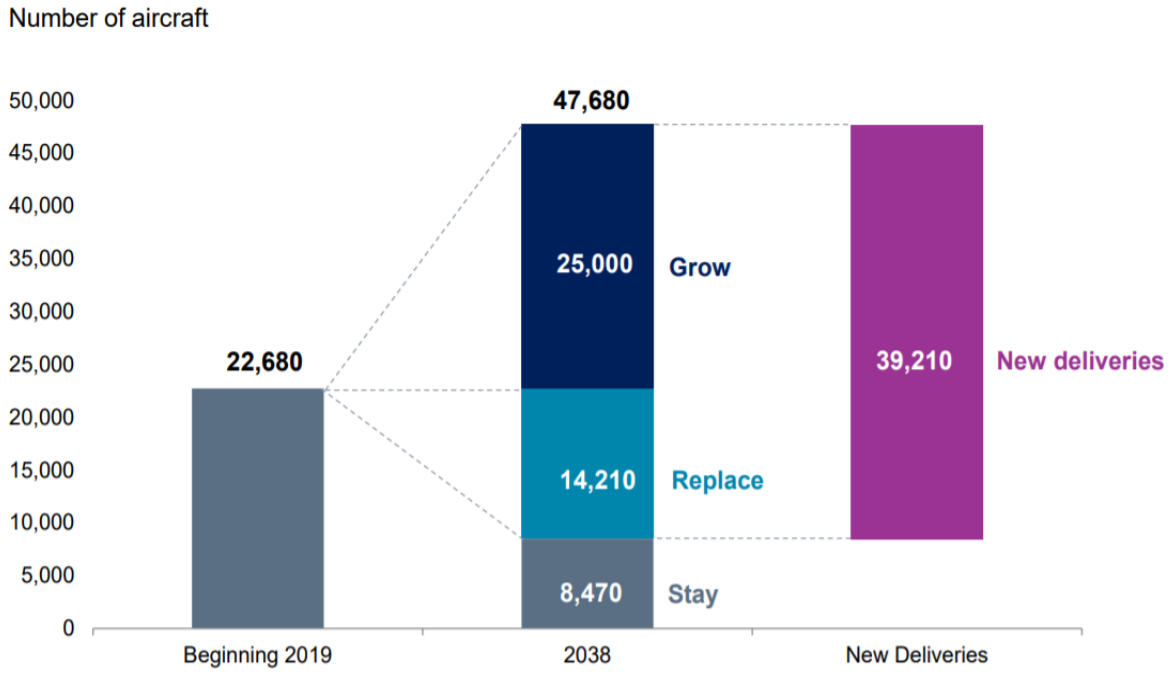

Figure 1.1: Expected growth for aircraft global fleet [3].

This rapid growth, coupled with the continuous increase in fuel prices and carbon emissions, which are expected to be up to 80% [4], have inspired research for a new alternative fuel that could supply the sector and reduce the environmental impact. Biofuels are attractive candidates due to its low greenhouse gases emission (GHG) and the decrease of the dependence on fossil fuel sources [5]. The use of biofuels can be a path to GHG reduction since most of the CO_2 released in burning the fuel would have been removed from the atmosphere while the plant was growing. Nevertheless, the environmental impact of the aeronautical sector exceeds the problem of the CO_2 emission because several pollutant agents are also produced during the fuel-burning process. These include soot, NO_x, unburned hydrocarbons and sulfur oxides, which have a negative impact on the air quality in areas near airports.

In the last 40 years, the fuel efficiency of jet aircraft has been estimated to be improved by more than 60% in terms of emissions of CO_2/passenger/km. Several improvements have come from step changes in technology, such as enhanced engine efficiency, airframe aerodynamics, and lighter materials, However the achievement of these ambitious goals remains challenging with current levels of Government and industrial investment in the relevant research and demonstration activities. As one approaches the theoretical limits, efficiency gains are much harder to achieve. This is the case with turbofan engines that can only be improved by up to 30% before theoretical limits are reached [4]. Other possible solutions may come from alternative fuels, that offer some advantages in the long term. The development of alternative fuels allows a faster benefit, as it is not constrained to the industrial assets of the aeronautical sector, in which the high investment costs slow the renovation of the production [4]. Moreover, the use of alternative fuels presents further advantages over the use of conventional jet fuel, as a reduced cost fluctuation, a worldwide homogeneous distribution of the feedstock depending on the alternative fuel production [5]. For these reasons, the contribution of alternative jet fuel is expected to grow by up to 30% by 2030 [1]. This poses a challenge because the aeronautical sector requires fuels with high energy density and with well-specified properties in order to comply with the current legislation. Any product proposed must be fully interchangeable with the existing jet fuel product to avoid the logistic problems of airports handling multiple fuels with varying qualities and the commercial limitations these would impose. For these reasons, the main research drive has been around the development of “drop-in” fuels, which can be used in the existing fleet, because the industry keeps its assets in use for around 40 years [1], due to the high investment costs.

One of the most promising candidates is a hydroprocessed vegetable oil (HVO) called NExBTL, which is a biofuel. This is a very promising fuel since it is already approved for blending ratios of 50/50 with conventional jet fuel and promotes less pollutant formation. Generally, running on a neat synthetic jet from hydrogenated processes reduces the emitted NOx by up to 12% [6]. This reduction in emissions while running on alternative fuels has been shown in engine demonstration flights. An excellent example was given by the Japan airlines that demonstrated

the feed-stock independence of hydroprocessed jet fuel through incident free operating of one of its Boeing 747-300. The roundtrip test flight operated one of four engines on a 50%/50% blend of conventional jet fuel and hydroprocessed biomass feedstock. The success of recent test campaigns has not only highlighted biomass product compatibility for gas turbines but also demonstrated the technological readiness and feedstock independence of the hydrotreatment process [7].

One of the biggest concerns with the use of alternative fuels has come from their low aromatic content. Seals in the aircraft and engine would leak if the aromatic content is lower than the specified values – the seals would shrink. For this reason, the aromatic content of synthetic fuel blends is currently fixed at a minimum of 8%. The performance of alternative fuels concerning particulate emissions has received considerable attention. Most works that evaluated biomass to liquid (BtL) or hydroprocessed renewable jet fuel (HRJ) has indicated a reduction in particle matter emissions. This is primarily due to the decrease in the aromatic content of the fuel. The main goal of this work is to study the burning characteristics of the different fuel mixtures, particularly to evaluate the effect of blending different amounts of HVO and JF in the burning behaviour of droplets to increase the knowledge on multicomponent fuels. Even though engine studies provide very useful information regarding fuel performance under realistic conditions, results can be dependent on several noncontrollable variables. On the contrary, in single droplet studies most parameters affecting the results are well known and controllable, and therefore the combustion characteristics observed are intrinsically attributable to the fuel.

1.2. State of the art

1.2.1. Engine emissions and environmental impact

In real combustion processes, air and fuel are mixed, ignited, and burnt to release heat. In ideal combustion, this process generates CO_2, water (H_2O) and sulfur dioxide (SO_2) depending on the fuel composition. However, real combustion is a multi-step process involving hundreds of intermediate reactions that affect the process and produce additional emissions. These additional emissions are usually considered pollutants, and include oxides of nitrogen (NO and NO_2) referred to as NOx, unburnt hydrocarbons (UHCs), carbon monoxide (CO), soot and sulfur oxides (SO_2, SO_3, and H_2SO_4) referred to as SOx. Figure 1.2 shows a schematic of the emissions from an aero engine. The amount of additional pollutants depends on the conditions in the combustion chamber (temperature, pressure, air-fuel ratios, and geometry of the combustor chamber) [4]. The international civil aviation organization (ICAO) regulates emissions with local air quality impacts (being the main ones NOx, UHC, CO, smoke, and SOx). CO_2 emissions are not regulated, but meeting customer demand for reduced fuel burn is already a key driver for

the industry and can outpace legislation, even though this reduction isn´t enough to achieve carbon neutral growth.

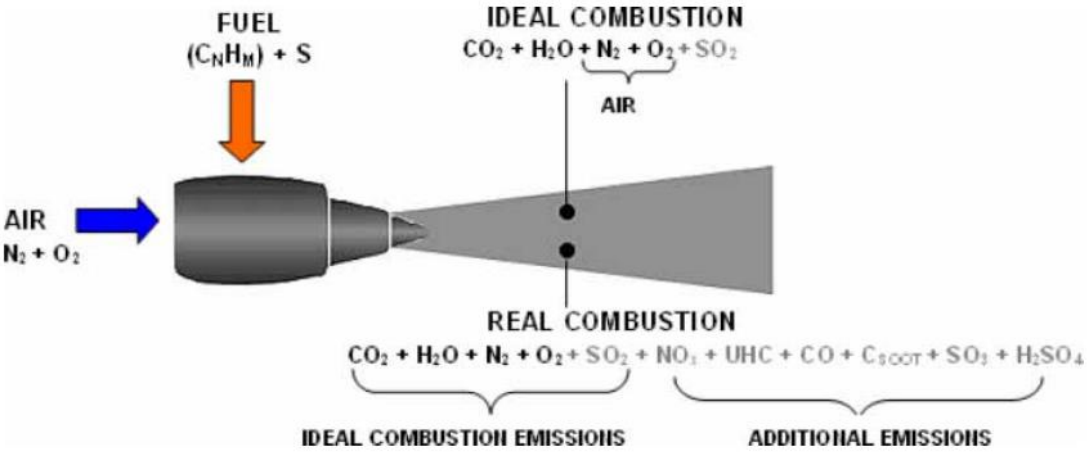

Figure 1.2: Schematic showing the ideal and real combustion processes for aero-engines [3].

NOx is formed from the oxygen and nitrogen in the air reacting at high temperatures in the combustor. The net effect of NOx on global warming is debated. Trough photochemical reaction in the troposphere it increases the tropospheric ozone [8] concentration and through liberating OH radicals it reduces the lifetimes of other GHGs such as methane (CH_4) [9]. The net result is thought to be a slight warming effect. The major impact and reason for legislation for emissions of NOx are due to its effects on local air quality near the airports.

SOx is a pollutant that contributes to the acidity of rainwater and generates health risks, but it is not considered a GHG. The source of SOx is the sulfur content in fuels. Aviation kerosene has sulfur contents much lower than coal and fuel oil because sulfur contents have a negative impact on the turbine lifetime. The reason for do not remove sulfur from JF is because it would require a more energy-intensive and expensive refining process and the addition of a substitute lubricant for the fuel system.

UHCs and CO are pollutants that contribute to the petrochemical smog and ozone creation at tropospheric levels. They are both products of incomplete combustion. Modern aero-engines have very low UHC and CO emissions, although work is ongoing to reduce them during starting and low-power idling.

Aviation's contribution to the tropospheric water vapor is very small compared to the natural hydrological cycle [10], but a aviation-induced warming effect is attributed to the fraction of H_2O transmitted into the much dryer stratosphere, where it is a powerful warming agent. Probably, more importantly, contrails can form from the engine exhaust at high altitudes, when the water crystallizes at very cold and wet ambient atmospheric conditions. Contrails can also

develop into cirrus clouds. These clouds trap outgoing longwave earth radiations at night, but in the daytime, they reflect sunlight. Their net effect may be a warming one, although difficult to quantify, this whole area remains one of great uncertainty and debate with the need for further quantitative research [4].

Figure 1.3 shows the radiative forcing (RF) components associated with aviation and a column that estimates the level of scientific understanding (LOSU). Over the years, several other studies have reported and updated the original estimates of the effects. RF is a measure of the change of energy balance of the earth's atmosphere system in watts per square meter. Positive values quantify the net warming effect, while negative values show a cooling effect. The net numbers from aviation still remain low when compared to the incident radiation from the sun of 342 W/m^2 [7].

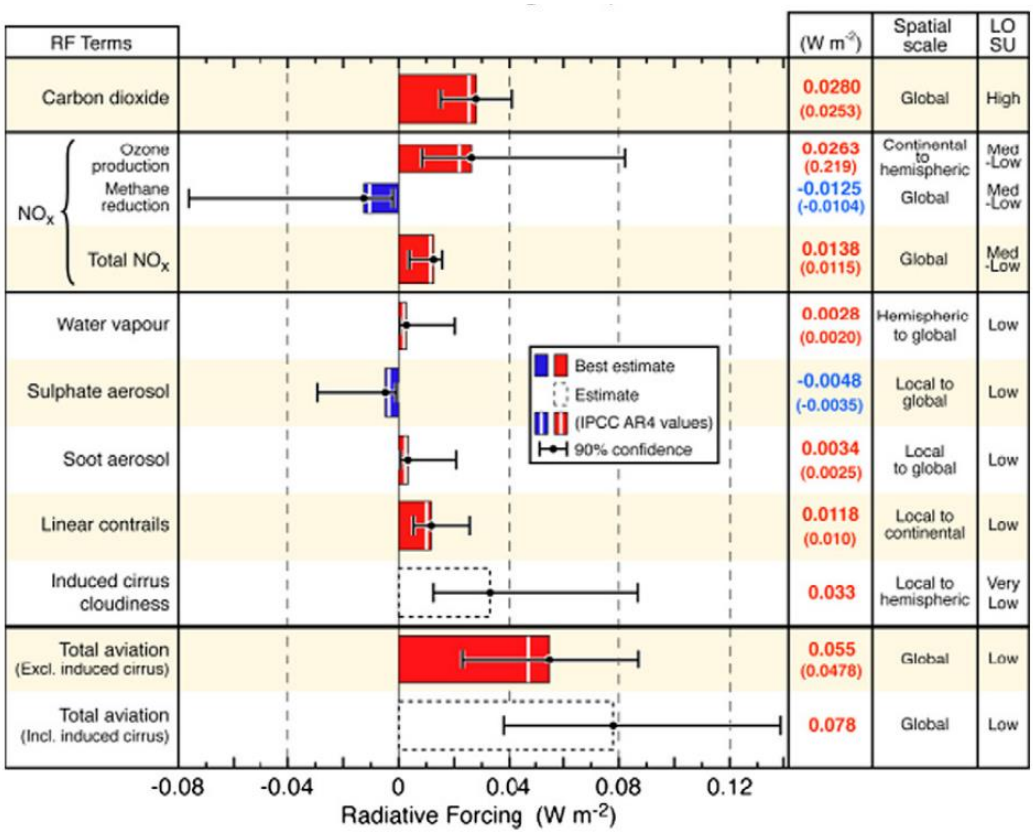

Figure 1.3: RF components associated with aviation. Bars show the best estimate available and include an estimate as to the confidence level in the data [7].

1.2.2. Fundaments of single droplet combustion

1.2.2.1. Droplet evaporation

Droplet evaporation involving heat and mass transfer processes in a turbulent environment has great importance for engineering applications, such as the atomization, and gas turbine engines evaporation and combustion of liquid fuels in internal combustion engines. In such applications, the liquid undergoes several processes before it becomes vapor, which then mixes with the oxidant and burns to release energy [11]. To achieve a better performance of these systems and reduce the emission of pollutants, the first step might be the fundamental study of the previous processes in order to develop models/methods that are able to predict accurately evaporation rates and burning rates. A spray may be considered as a cloud of droplets, which are produced through the disintegration of a liquid jet issuing from a simple cylindrical nozzle or more complex injectors. It was shown that in the near fields of the injector tip, a dense region of ligaments and droplets having various sizes might occur, while on the far field, a dilute region of more uniform droplets. Interactions between droplets prevail in the dense region, while the aerodynamic transport of droplets is dominant in the dilute dispersed spray region. In spray combustion, the droplet vaporization rate is the dominant controlling factor of combustion. This conversion (liquid to vapor) can be referred to as boiling or as evaporation. Boiling occurs when the submerged surface needs to be heated to an above boiling temperature of the liquid. Evaporation occurs when the liquid is above boiling temperature or in the presence of a mix between incondensable gas and vapor.

Figure 1.4 shows a schematic of a single droplet burning. In this process, mass and heat are transferred between the droplet and surrounding gas. Heat is transferred to the droplet surface by conduction and convection through the hot gas surrounding the droplet. Heat and mass transfer is affected by the droplet Reynolds number. Vaporization rates are affected by several factors such as temperature, pressure, fluid properties, surrounding gas properties, droplet diameter and droplet velocity relative to the gas. Depending on the locations in the spray, neighboring droplets might affect the vaporization rate in the spray. However, in spray evaporation and combustion computations, it is generally assumed that the overall spray behavior can be obtained by the summing behavior of individual isolated droplets surrounded by a gas phase that itself has varying properties. Even when the assumption that droplets behave as if they were isolated from each other is not satisfactory, the behavior of a single isolated droplet in an oxidizing environment will provide fundamental input to the overall spray analysis. From a practical point of view, the vaporization and combustion of single droplets are very important in understanding spray flows. The reason for its intensive investigations is that these relatively simple phenomena may be used to advance the knowledge of the complex mechanism of two-phase spray combustion encountered in liquid-fueled combustion systems.

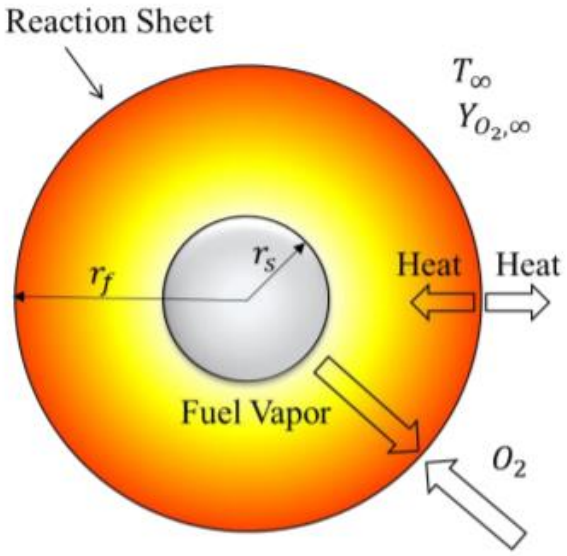

Figure 1.4: Schematic of a single droplet burning.

1.2.2.2. Basic evaporation/combustion model

The basic droplet vaporization/combustion theory for an isolated single-component droplet in a stagnant environment was proposed by G. Godsave [12] and Spalding [13]. In this model, it is assumed that the droplet is spherical, the boiling point of pure fuel is well known, and radiation heat transfer is negligible – these assumptions are valid except for conditions of very low pressure or highly luminous flames.

After an initial transient period, steady-state evaporation is established from an analytical solution referred to as the "D^2 law" [12]. In this solution, the droplet squared diameter diminishes linearly with time according to:

$$d_0^2 - d(t)^2 = Kt \quad (1.1)$$

This analytical solution is sometimes simply called the "D^2 law" of droplet evaporation, K is known as the evaporation constant given by:

$$K = \frac{8\lambda_g}{\rho_{liq} c_{p,g}} \ln(B_{q+1}) \quad (1.2)$$

where $c_{p,g}$ represents the specific heat at constant pressure and λ_g represents the thermal conductivity. Experiments shows that "D^2 law" is valid after an initial transient period associated with droplet heating until a value near the boiling point.

Once the initial diameter of the droplet is known and the evaporation constant (K), the "D^2 law" is able to predict the droplet evaporation time, also known as the droplet lifetime (t_d), as follows:

$$D^2(t_d) = 0: \quad t_d = \frac{D_0^2}{K} \qquad (1.3)$$

Note that to use the previous equations it is required to know the mean values for the properties $c_{p,g}$ and λ_g, which are present in the evaporation constant K [14].

Three parameters are generally evaluated: the mass burning rate (evaporation), the flame position above the fuel surface, and the flame temperature. The most important parameter is the mass burning rate that permits the evaluation of the so-called evaporation coefficient, which is most readily measured experimentally where D_0 is the original drop diameter and D the drop diameter after time t,

$$D^2(t) = D_0^2 - Kt \quad (1.4)$$

1.2.2.3. Effects of ambient temperature

The ambient temperature is a significant factor because it affects evaporation rates, ignition and heating time. The significance of this parameter is addressed in this work.

Figure 1.5 shows the effect of ambient temperature in the ignition delay of a n-heptane droplet. High ambient temperature promotes droplet evaporation by providing enhanced heat transfer to the droplet surface, while allowing faster evaporation of the fuel components. This effect was observed in [15]. Authors made several numerical studies for n-heptane and concluded that the evaporation rate and burning rate showed a strong dependence on the ambient temperature, increasing monotonically with the ambient temperature. This phenomenon was also observed by [16]. Another very important factor affected by the ambient temperature is the ignition delay time. Several authors stated that the increase in ambient temperature leads to a decrease in ignition delay time [17].

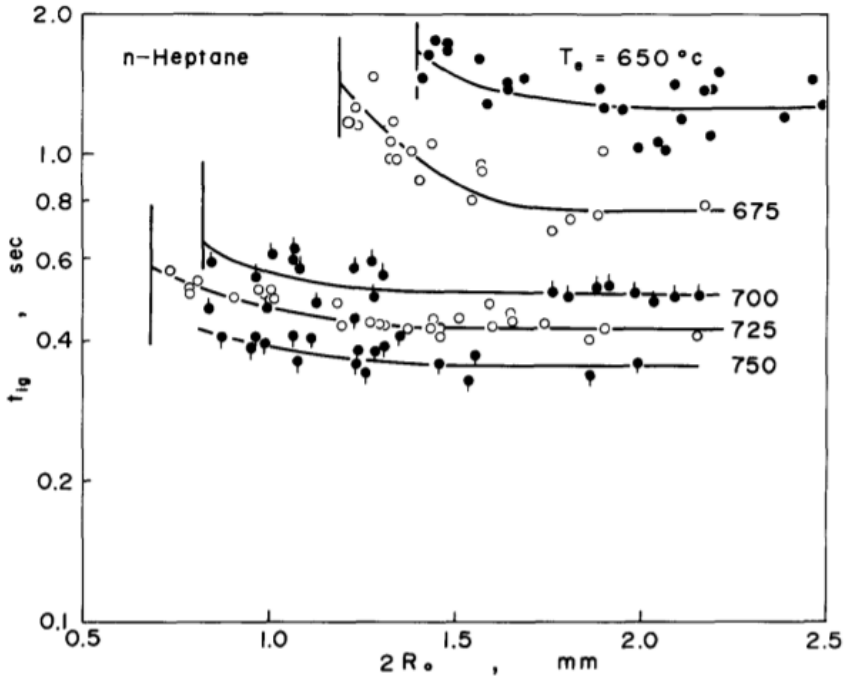

Figure 1.5: Measured ignition delay time versus droplet diameter for n-heptane droplets for different ambient gas temperatures [17].

From the previously works from other authors, it was observed that the kerosene droplets followed the "D^2 law" after a heating period and that the ambient temperature was a very important parameter, which greatly affected ignition and combustion phenomena.

1.2.2.4. Effects of forced convective flow

This section refers to the effects of forced convection on ignition delay and evaporation rate. In contrast with studies under stagnant conditions, there has been limited research on droplet ignition under convective conditions. Whang et al. [18] conducted an experimental study of the ignition of a suspended droplet in the convective post-flame environment of a flat-flame burner. The ignition delay and location were measured for n-heptane and n-hexadecane droplets for a range of ambient temperatures, droplet diameters, and droplet Reynolds number (Re_D). Their results indicated that the minimum ambient temperature for ignition increases significantly due to forced convection. Despite the different results in the literature, it can be concluded that the ignition location and flame development are strongly influenced by Re_D. As Re_D increases, the ignition location moves from the front to the wake of the droplet, and correspondingly an envelope flame changes to a wake flame. Further increase in Re_D leads to either no ignition or flame extinction [18]. Forced convection was found to impede droplet ignition in that the minimum ignitable gas temperatures were higher compared with natural convection [18]. Sangiovanni [19] states that for droplet spacings in excess of twenty droplet diameters convection reduces the ignition delay times [12].

1.2.2.5. Burning clouds

Each droplet in a cloud has a gas film surrounding it. The local ambient conditions are defined as the gas properties at the edge of the gas film but within the volume of the cloud. This definition becomes imprecise when the gas films of neighboring droplets overlap. In such case, the local ambient conditions would be replaced with some average over the gas in the droplet neighborhood [13,19]. Despite numerous analytical and experimental studies on burning droplet arrays, the current understanding on burning of clouds and sprays is still limited. Figure 1.6 shows a schematic of the different regimes of droplet interactions, and how they are affected by the group combustion number, G. The primary consideration in most studies has been the effect of droplet separation on the overall burning rate. An interesting approach to the spray problem has been suggested by Chiu and Liu [20] that consider a quasi-steady vaporization and diffusion process with infinite reaction kinetics. They show the importance of G, which was derived from extensive mathematical analyses as:

$$G = 3\left(1 + 0.276 Re_D^{\frac{1}{2}} Sc^{\frac{1}{2}} LeN^{\frac{2}{3}}\right)\frac{R}{S} \qquad (1.5)$$

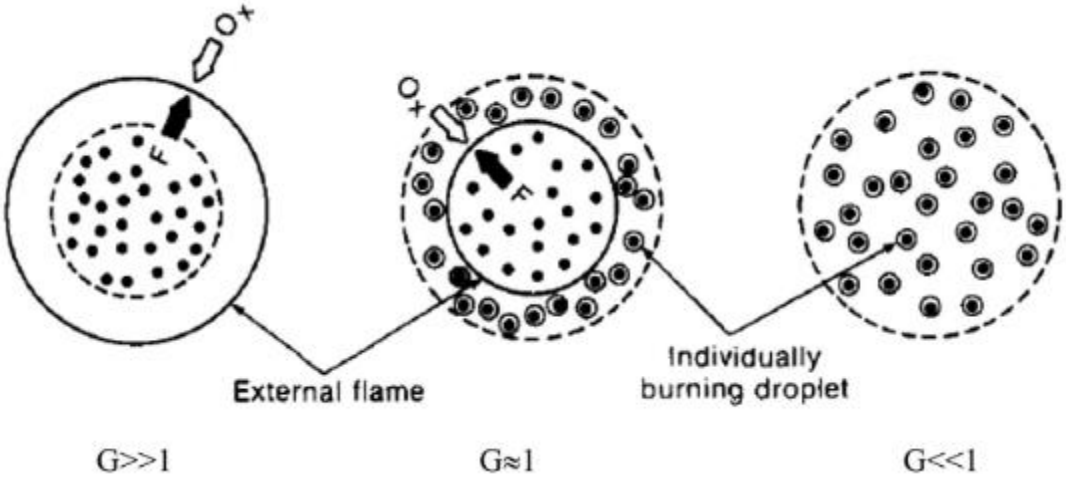

Figure 1.6: Schematic of Inter droplet interaction [19].

where Re, Sc, and Le are the droplet Reynolds number, the Schmidt number, and the Lewis number, which are presented in annex 1. In Eq. (1.5), N is the total number of droplets in the cloud, R the instantaneous average radius, and S the average spacing between droplets. The value of G was shown to have a profound effect on the flame location and distribution of temperature, fuel vapor, and oxygen. Four types of behaviors were found for large G numbers. External sheath combustion occurs for the largest value. As G decreases, there is successively external group combustion, internal group combustion, and isolated droplet combustion. Isolated droplet combustion obviously is the condition for a separate flame envelope for each droplet. Typically, a group number less than 10^{-2} is required. Internal group combustion involves a core with a cloud where vaporization exists such that the core is surrounded by the

flame [21] – this happens for G values above 10^{-2} and somewhere below 1. As G increases, the size of the core increases. When a single flame envelops all droplets, external group combustion exists. This phenomenon begins with G values close to unity (many industrial burners and most gas turbine combustors work in this range). With external group combustion, the vaporization of individual droplets increases with distance from the center of the core. At very high G values (above 10^2), only droplets in a thin layer at the edge of the cloud vaporize. This regime is called the external sheath condition [21].

1.2.2.6. Multi-component fuel droplets

There are various complications that occur when a multicomponent liquid is considered since different components vaporize at different rates, creating concentration gradients in the liquid phase and causing liquid-phase mass diffusion [13]. Due to this, the more volatile substances tend to vaporize faster at first until their surface's concentration values diminished and further vaporization of those quantities becomes liquid-phase mass diffusion controlled. Mass diffusion in the liquid phase is of primary importance in the vaporization process for a multi-component fuel. At first, early in the droplet lifetime, the more volatile substances in the fuel at the droplet surface will vaporize leaving only the less volatile material that evaporates more slowly. More volatile material still exists in the droplet interior and will tend to diffuse toward the surface because of concentration gradients created by prior vaporization. This diffusion is balanced by the counter diffusion of the less volatile fuel components toward the droplet interior [16]. Classical droplet vaporization theory treats spherically symmetric, quasi-steady, single-component, isolated droplets. It is on the relaxations of these features where modern developments are concentrating. In real combustors, the local field around a droplet is not spherically symmetric but multi-dimensional; also, transient effects are significant. Real fuels are multi-compositional with varying volatilities of the components [16].

1.2.2.7. Influence of inter-droplet spacing

The inter-droplet spacing has great importance on the burning rates, ignition delay time, and flame position. Figure 1.7 shows the influence of droplet spacing in the ignition delay times. As the distance between droplets becomes larger, the influence of neighboring droplets becomes smaller – the transport and aerodynamic characteristics tend to the values of isolated droplets. On the contrary, if the space between droplets decreases, they cannot be treated as isolated droplets; the neighboring droplets are within the gas film or wake of the droplet. In a convective situation, a droplet can influence a second droplet at a distance of many tens of droplet radii if the latter is in its wake [13]. Sangiovanni discusses the various effects of the inter-droplet spacing in its experimental work [19]: the fuel droplet ignition delay times for small droplet spacings can be substantially greater than the delay times for isolated droplets; for small droplet spacings, the role of forced convection in heating and vaporizing droplets as a result of droplet/gas relative velocity becomes insignificant since each droplet travels in the wake of a

preceding droplet; and the effect of droplet interaction on the ignition process becomes more important for small droplets, low gas-phase temperatures, and fuels with low volatility.

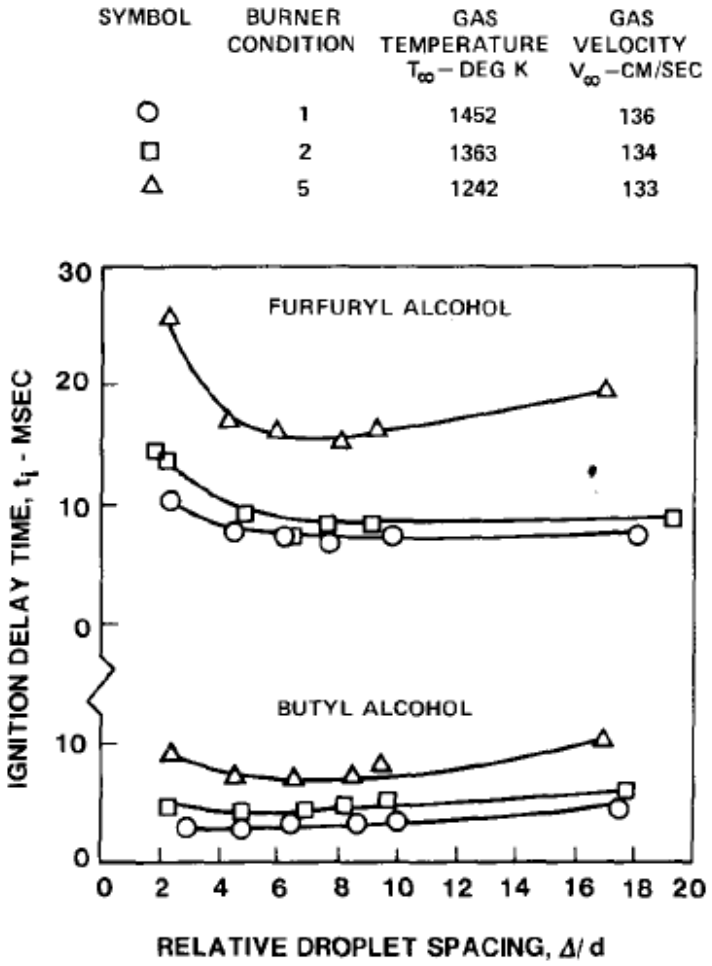

Figure 1.7: The influence of droplet spacing in the Ignition delay time[].

1.2.2.8. Physics of puffing and micro explosions

The combustion of a highly multicomponent fuel or of an emulsion of two fuels with different volatility usually leads to the occurrence of puffing, and micro explosions. Figure 1.8 illustrates the occurrence of puffing and micro explosions. Initially, small gas bubbles start to nucleate inside the fuel droplets, and the pressure inside the vapor bubble becomes higher than the ambient pressure. The tiny bubbles coalesce into a relatively larger bubble due to the internal circulation inside the droplet, and thus larger gas bubbles are formed. Since the nucleation sites are dependent on the proportion of higher volatile components, a lower proportion of the higher volatile component results in fewer nucleation sites and, hence, less coalescence of tiny bubbles. Therefore, the bubble cannot grow further and eventually breaks apart resulting in the ejection of small secondary droplets. The breakup of a relatively smaller bubble without droplet breakup is referred to as puffing. The breakup of the inner gas bubble can lead to the

breakup of the fuel droplet, leading to the ejection of the smaller secondary droplets and volatiles. The complete breakup is called micro explosion and can be associated with a flame involving the ejected material [22]. The appearance of puffing and micro explosions during the overall droplet lifetime can also be referred to as disruptive burning.

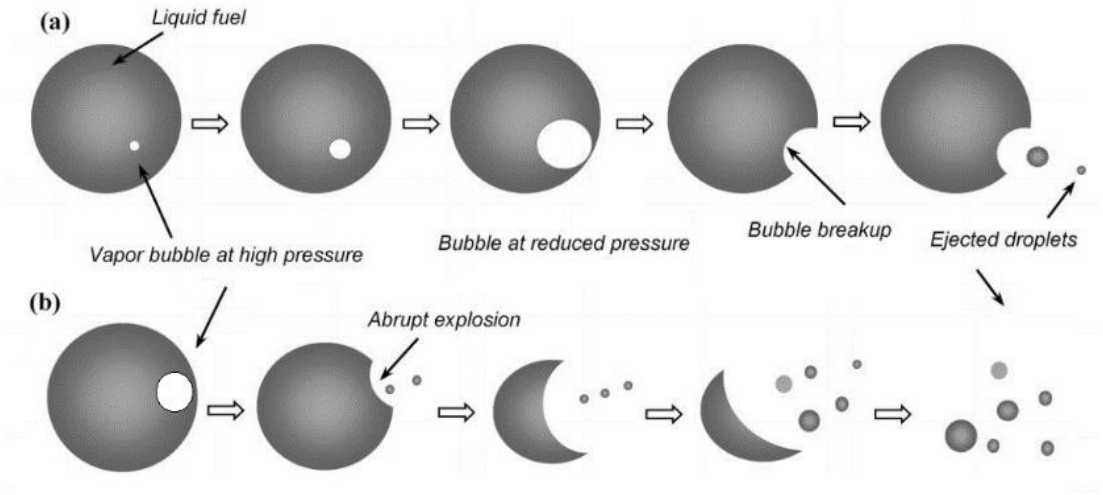

Figure 1.8: Sequence regarding nucleation, bubble growth, and the breakup of parent droplet: (a) Schematic of puffing; (b) Micro explosions.

The initiation, development, and effect of these processes on the multi-component fuel droplet combustion need to be further comprehended. Considering the microscopic size of the fuel droplets within the real spray, studying these processes during spray combustion is quite challenging. Alternatively, these processes can only be extensively investigated using an isolated fuel droplet undergoing combustion. Magnified visualization of the droplet surface and the surrounding environment during combustion will provide more in-depth details about the occurrence of puffing and micro explosion.

1.3. Alternative jet fuels

In this section, the topic of alternative fuels in the aeronautical sector is addressed. In non-aviation sectors, the use of alternative fuels with different properties or phases is allowed through a small and justified engine upgrade (for example, in the automotive industry), but in the aviation sector there are great restrictions to the use of alternative fuels for various reasons. Firstly, an optimum operation of gas turbines requires specific and well-defined fuel properties due to the extreme conditions of operation and conditions of combustion, which reduces the range of suitable candidate fuels to a restricted group of liquid hydrocarbon blends. Moreover, the alternative fuel must be interchangeable with the present jet fuel, and therefore compatible with the existing fleet. If not, airports would have to provide different qualities of fuels, introducing logistic issues, and limiting the movement of the aircrafts towards the

destinations where the alternative refueling is available [7]. Because of this second requirement, alternative fuels for aviation are also referred to as “drop-in” fuels. Fossil fuel prices are becoming more volatile day by day. So, it is essential to introduce alternative aviation fuels generated from renewable resources, especially biomass [23]. Alternative fuel is, therefore, suitable for aviation if it presents similar properties to conventional jet fuel, especially in terms of heating value and chemical properties [1]. So, in this chapter, a comparison between the available alternative jets fuels will be addressed in order to evaluate what kind of alternative jet is suitable for the aviation sector. Figure 1.9 shows different fuels in terms of their lower calorific value (LCV) as a function of their density. The figure includes different fuels ranging from conventional HC to alternative fuels obtained from different production methods and feedstocks. The horizontal line in Figure 1.9 represents a constant LCV of 42.8 MJ/kg. This value is currently in use as the minimum limit for aviation fuels. The two vertical lines in the figure show the current specification limits for jet fuel density of 775-840 kg/m^3. In industrial gas turbines, fuelled by gaseous fuels, the Wobbe index has been used to identify how far away from the design fuel an alternative fuel can be [23]. This considers the mass flow of the fuel, along with the amount of energy, that will be delivered through a given fuel delivery system to ensure that the fuel placement is correct. The Wobbe index, I_w, is defined as:

$$I_w = \frac{LCV}{\sqrt{SG}} \quad (1.6)$$

Figure 1.9 also shows lines of constant Wobbe index. The Wobbe index needs to be modified for use with liquid fuels, being the situation more complex with the liquid fuel properties such as surface tension, viscosity, etc. having a substantial impact on fuel atomization [7].

A high LCV and high density would be most desirable for flight, offering the maximum energy release per volume and mass unit. A line has been added to the hydrocarbon group in Figure 1.9 showing the clear trade-off between high energy densities and low “mass” densities, and the upper limit to the desirability of high LCV and high-density using hydrocarbons. In general, heavy fuels have high energy densities and light fuels have high specific energy.

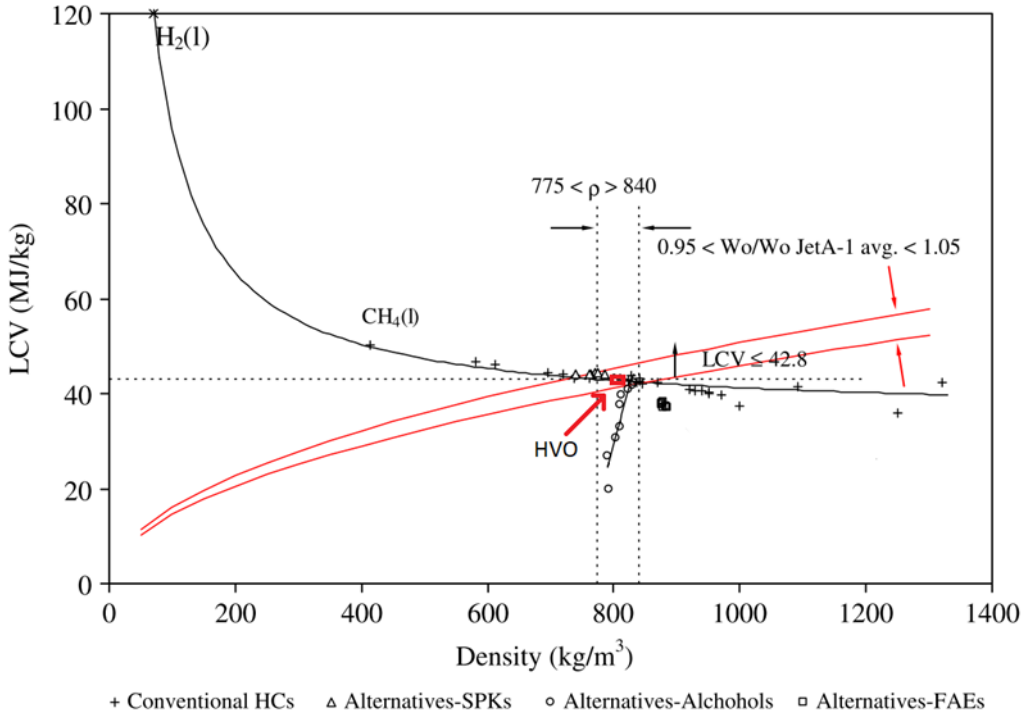

Figure 1.9: Lower calorific value as a function of density for a range of liquid fuels [7].

FAEs, commonly referred to as biodiesels, are most likely to be long-chain fatty acid ester groups derived from the transesterification of the triglyceride fat groups in the base oil. Figure 1.10 illustrates the transesterification process. The exact composition of this fuel is dependent on the composition of its original oil and how it's processed by the transesterification method. This fuel can be separated into two groups, by using methanol or ethanol will produce methyl (FAME), and by using ethyl esters it will produce (FAEE). The fuel properties depend on the raw material. Transesterification is potentially a comparatively cheap way of converting the large, branched molecular structure of the bio-oils into smaller, straight-chain molecules of the type required in regular diesel combustion engines. The use of biodiesel as aviation fuel does not require engine modification and infrastructure, but it presents some disadvantages that make FAE not suitable for the aviation sector. Its use reduces aircraft efficiency. The biodegradability of biodiesel may cause biological growth during storage which will affect stability [24]. The freezing point of biodiesel is very high compared to petroleum-based aviation fuel, which makes it insufficient for high altitude flights.

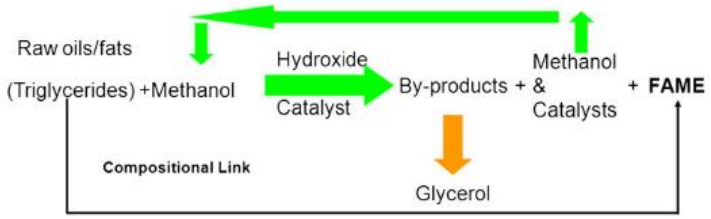

Figure 1.10: Transesterification process.

Fischer-Tropsch fuels (FT fuels) are hydrocarbon fuels, which are produced by catalytic conversion of syngas (CO and H2) [23]. Direct conversion of feedstock into a product (also known as liquefaction) is the most energy-efficient route, but presently commercial technology is based upon indirect conversion [23]. Figure 1.11 illustrates the FT process, which requires the production of syngas from a suitable feedstock that is then fed into a liquid conversion process. Depending on the feedstock used, the process is entitled 'anything too liquid' (XtL), where 'X' is 'C' (coal), 'G' (gas) or 'B' (biomass). Figure 1.11 shows the production method for this fuel. Firstly, syngas is produced through gasification of coal or biomass. The FT requires syngas and involves carbon chain building [25]. The synthetic crude yield is then upgraded by hydroprocessing–cracking and to produce a commercial product, thereby allowing the refinery to effectively design a fuel-based upon the desired chain lengths. The characteristic of the FT fuel is more independent of the feedstock and depends on the operating conditions such as temperature, pressure and syngas composition of the FT process. This is a major advantage because it is possible to control the output carbon numbers of the process and develop synthetic kerosene suitable for aviation [25]. However, this process is expensive, and the efficiency of the process varies from 25% and 50%, and these fuels tend to offer low power and low fuel economy due to less energy density. New fuel generations are being developed and several agencies such as DLR and NASA, have been developing and testing new generation FT fuels [26].

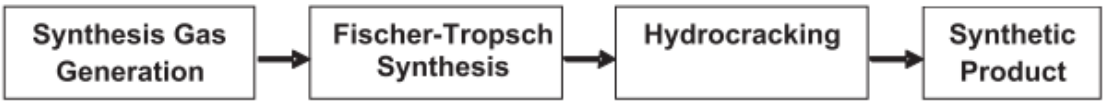

Figure 1.11: FT production process.

Synthetic paraffinic kerosene from hydroprocessing of esters and fatty acids (HEFA) is also referred to as hydroprocessed renewable jet fuel (HRJ) and, whenever animal biomass is not involved, as hydroprocessed vegetable oil (HVO). The suitable feedstock for HEFA production is fat biomass, rich in glycerides (mainly triglycerides), free fatty acids and fatty esters. The existing production plants mainly convert camelina oil, jatropha oil, and algae as energy crops, cooking oil and animal fat as side products of other industrial chains [23]. Figure 1.12 illustrates the productive process of HEFAs. After a first pre-treatment, aimed to remove impurities from

the feedstock, the biomass is refined through three main hydroprocessing stages. The objective of the hydrotreatment is to convert the biomass into paraffins. Oxygen is removed in presence of excess hydrogen via hydrodeoxygenation and decarboxylation processes, along with nitrogen, sulfur and residual metals. Selective hydrocracking is necessary to reduce the paraffins carbon number to a suitable value for aeronautical applications, namely C8-C16. The presence of this stage marks the difference between the production processes of hydroprocessed jet fuel and diesel fuel, which is referred to in this case as biodiesel. Then, in the isomerisation, the paraffins are converted into more compact isoparaffins, reducing the hydrocarbon blend freeze and flashpoints. These reactions are empowered by a multifunctional catalyst. The HRJs present several benefits such as being free of aromatics and sulfur and possess high cetane number, high thermal stability and low tailpipe emissions [27]. These fuels are stable for storage and resistant to microbial growth. HRJs are suitable for conventional aircraft engines without further engine modification and do not raise any fuel quality issues. These fuels avoid the chance of deposit formation in the engine and engine corrosion [28]. The fuel combustion is completely ash-free. HRJs are highly fit for higher altitude flights because of the better cold flow properties in comparison to other alternative fuels [29]. Additionally, the whole production process can easily be integrated into a conventional oil refinery, avoiding the development cost of a dedicated plant [1].

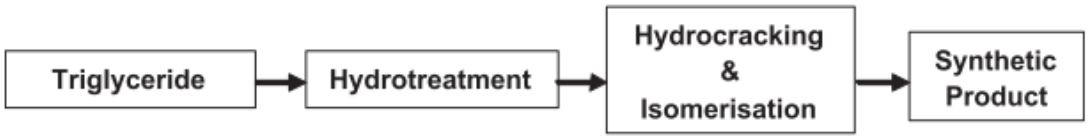

Figure 1.12: Hydroprocessing of vegetable oil.

1.4. Jet fuel

Aviation turbine fuel, commonly known as jet fuel (JF), is a distillate of the kerosene type, refined from conventional petroleum sources specially designed for gas turbine applications in the aeronautical industry. As gasoline and diesel fuel, JF is mainly composed of paraffins, naphthenes, and aromatics, along with small amounts of olefins and other compounds. The jet fuel composition is addressed in chapter 2. This wide variation in compounds found in jet fuel causes the combustion engineer difficulties when trying to model any combustion process. It is enriched with several additives, aimed to inhibit the hazard of static charges, reduce the oxidizing and corrosive potentials, increase the lubricity and improve the cold flow properties. The presence of additives, even though in parts per million, marks the main difference between jet fuel and kerosene [7].

The composition presents intermediate values for both vapor pressure and octane number, which result as the best values for the stable combustion under the extreme conditions of the turbine engine. Moreover, the high flash point reduces the explosion hazard, while the low freeze and wax points allow the high-altitude flight.

The main jet fuel grades for civil aviation applications are Jet A and Jet-A1. Jet A is only supplied for domestic flights in the USA, while Jet-A1 is adopted in the rest of the world. The two grades present similar properties, and mainly differ in the freezing temperature: -40 and -47 °C for the A and A1 grades, respectively.

The American standard specification ASTM D1655 [30] defines both A and A1 grades, while the European standard specification DEF STAN 91-91 [31] only defines the A1 grade, with slight and more stringent exceptions.

1.5. Overview

Only HVO (HEFA) and BTL (FT) fuels provide scope for GHG emissions reduction, with HVO offering reductions of 40% to 90% and BTL from 60% to 90% over their lifecycle, compared with conventional oil-derived fuels [32]. These results, however, assume 100% HVO or BTL which may not meet the specification in all properties [32]. It is important to mark the difference between the alternative jet fuel (the final mixture) and the alternative blending component. The standard specification for unconventional jet fuels – ASTM D7566 [33] – does not allow the direct use of the second. In order to further guarantee the fuel fitness, the alternative blend is constrained to consist of at least 50 %V of conventional jet fuel. The implementation of biofuels is supported by the growing supply of algal oil, HVO could constitute a significant share of transport fuels by 2030, with production in the order of 25 Mt/y, and in the order of 60 Mt/y by 2050 [32]. By comparing HVO with other alternative fuels it can be said that it provides one of the best solutions in terms of environmental impact, and in terms of backward compatibility as it was previously stated and in terms of production capability. So, for this work, a HVO with commercial name NExBTL, produced by NESTE, is used due to its properties and the potential to become an alternative to fossil fuels.

1.6. Objectives of this work

The objective of this work is to study the ignition and combustion characteristics of single droplets of jet-A1 (JF), hydroprocessed vegetable oil (NExBTL) and their mixtures in a drop tube furnace (DTF). Jet-A1 is used as a reference fuel for this work because it is the most common fuel used in the aviation sector, and HVO has been chosen due to its potential as a biofuel and because it is approved for blending with jet fuel in 50%/50% ratios. To evaluate the effect of blending HVO with jet fuel on the ignition and combustion characteristics of the

resulting mixtures, three mixtures of these two fuels were burned in a drop tube furnace with controlled wall temperature and oxygen concentrations.

Chapter 2

2. Materials and methods

This chapter describes the materials and methods used during the work. Firstly, the experimental setup is introduced. Next, the methods used are described. Finally, the properties of the fuels used are summarized.

2.1. Experimental setup

Figure 2.1 shows the experimental setup used in this study. It is composed by a DTF (drop tube furnace) and auxiliary equipments.

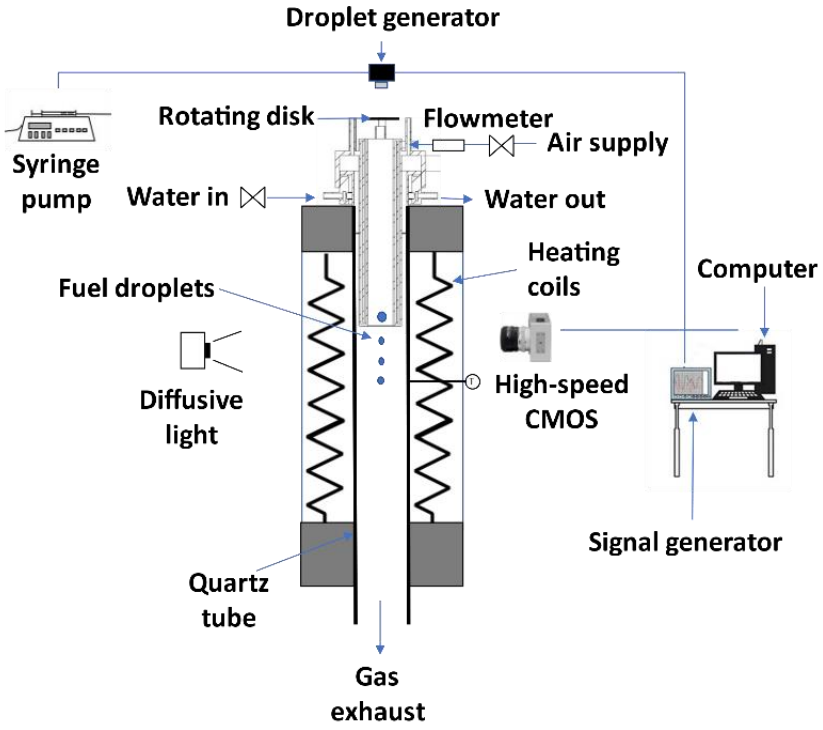

Figure 2.1: Schematic of the experimental setup.

2.1.1. Experimental facility

In order to study single droplet ignition and combustion, a new setup was projected and built. The DTF used in this experiment was designed for studies using solid biomass. So, a new injector for liquid fuels was developed. The water-cooling system and the air supply were designed similarly to the previous solid fuel injector for interchangeability between them in the same DTF.

The new injector was designed in CAD and is shown in figures 2.2, 2.3 and 2.4. During the design of the injector, several restrictions were considered. The main restrictions were in terms of inner diameter due to some fuel contamination in the inside walls. This creates safety issues due to the appearance of an updraft flame. The length of the tube is also a limitation because the droplet travel distance should be the minimum possible in order to minimize droplet heat up inside the injector and avoid ignition inside the injector. The injector was designed with a water-cooling system in order to maintain a good temperature for the operation of the setup without getting damaged and to avoid ignition inside the injector. The air supply is also a very important factor in order to have an airflow inside the drop tube with the minimum turbulence intensity possible, so a series of screens and nets where place to align the flow and reduce the maximum eddy diameter. A net with a 50 μm diameter and a honeycomb with 0.6 cm diameter and 6 cm length were used. The air supply was 5.7 l/min with a precision error of ±2%. The injector was built in the workshops of Instituto Superior Técnico using stainless steel 304. This material was chosen due to its resistance to corrosion and affordable price. It contains 18% chromium and 8% nickel. Figures 2.5 and 2.6 show the different parts of the injector. The injector was built in 3 separate parts in order to facilitate construction, cleaning and to allow different arrangements of screens and nets.

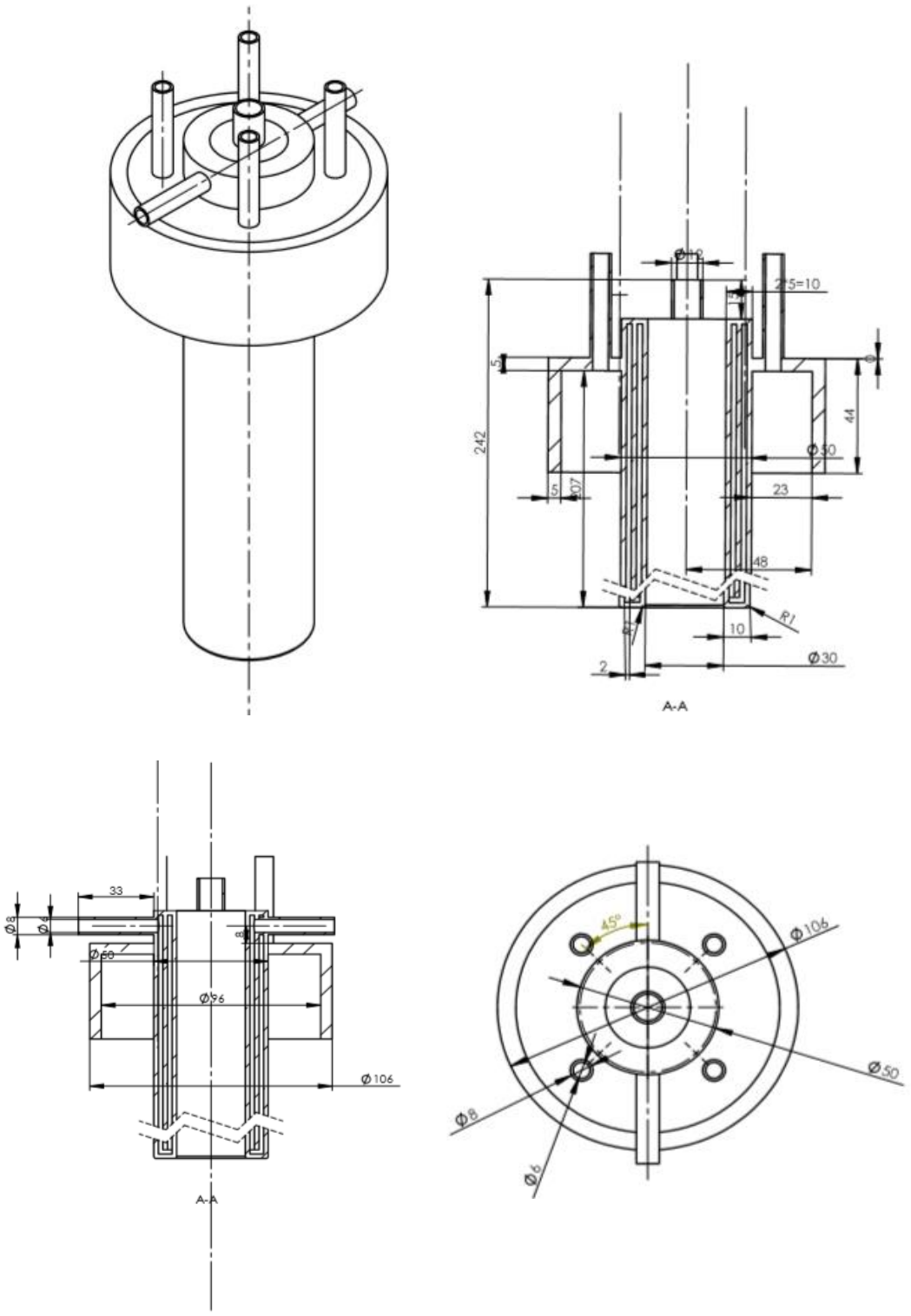

Figure 2.2: Technical draw of the injector – part 1 (dimensions are in mm).

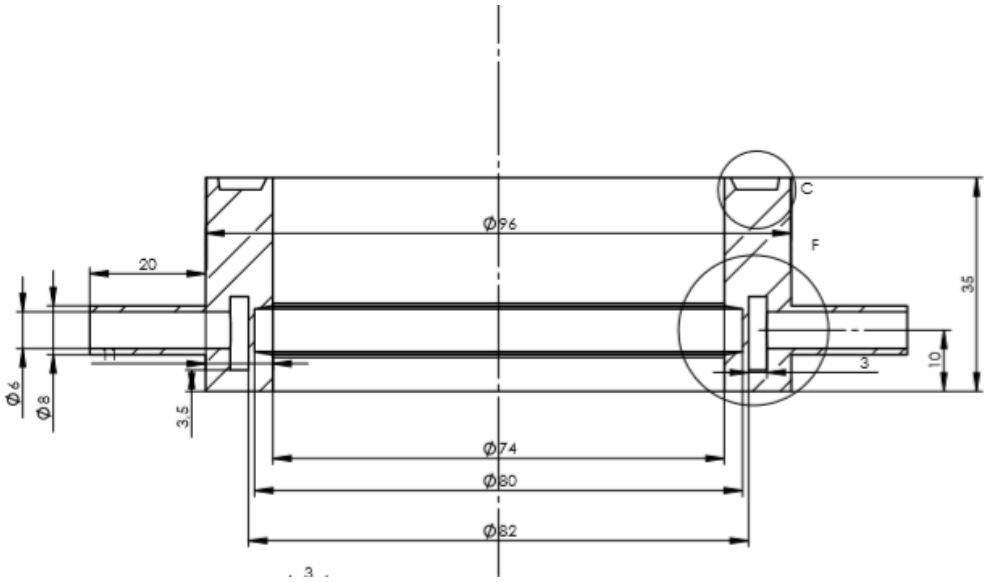

Figure 2.3: Technical draw of the injector – part 2 (dimensions are in mm).

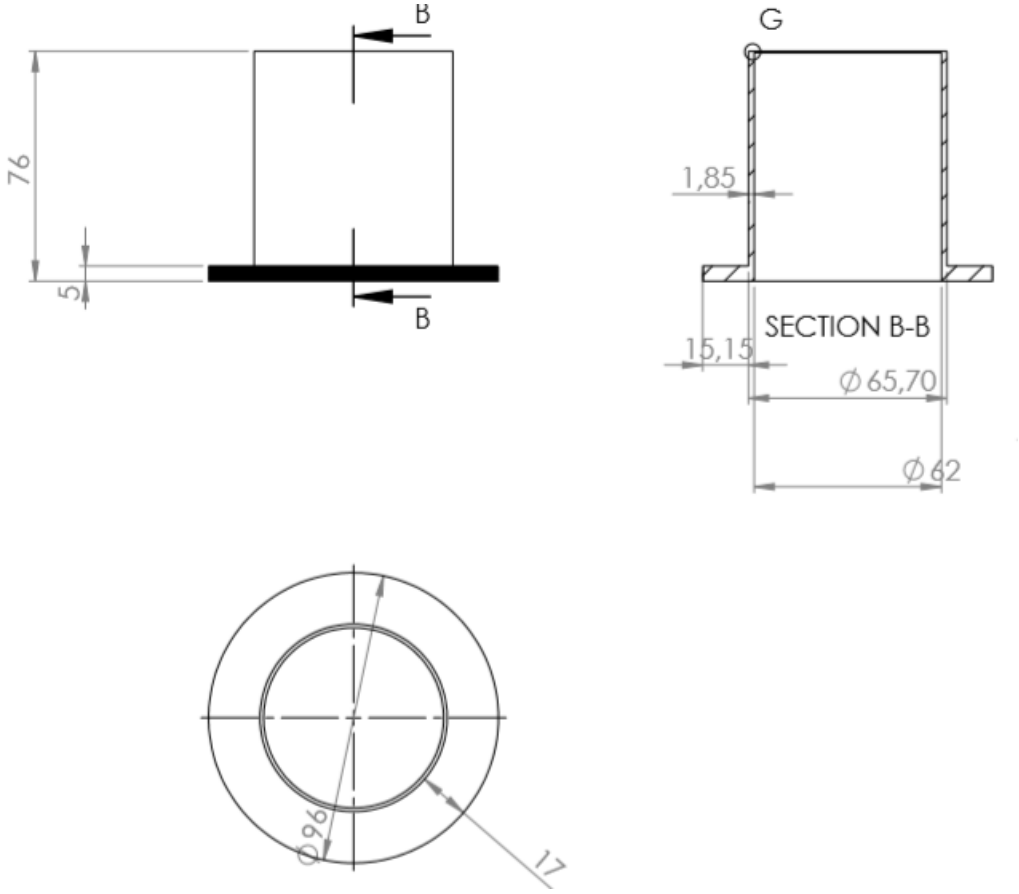

Figure 2.4: Technical draw of the injector – part 3 (dimensions are in mm).

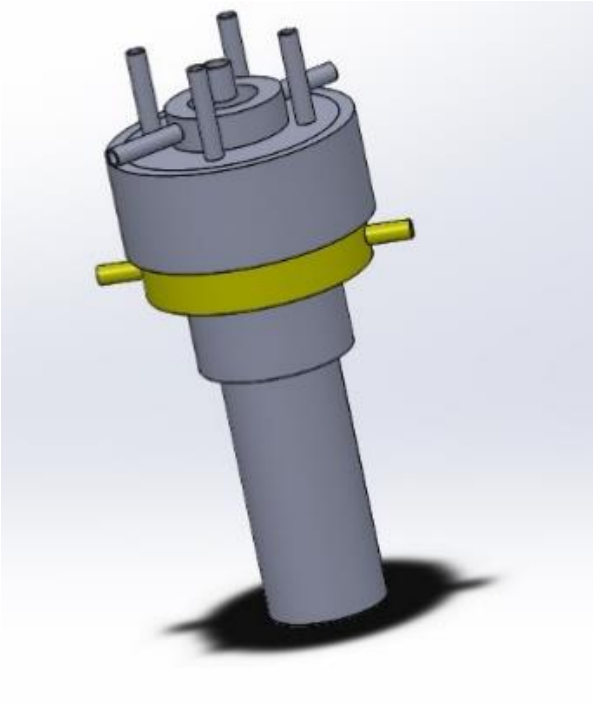

Figure 2.5: Fully assembled injector.

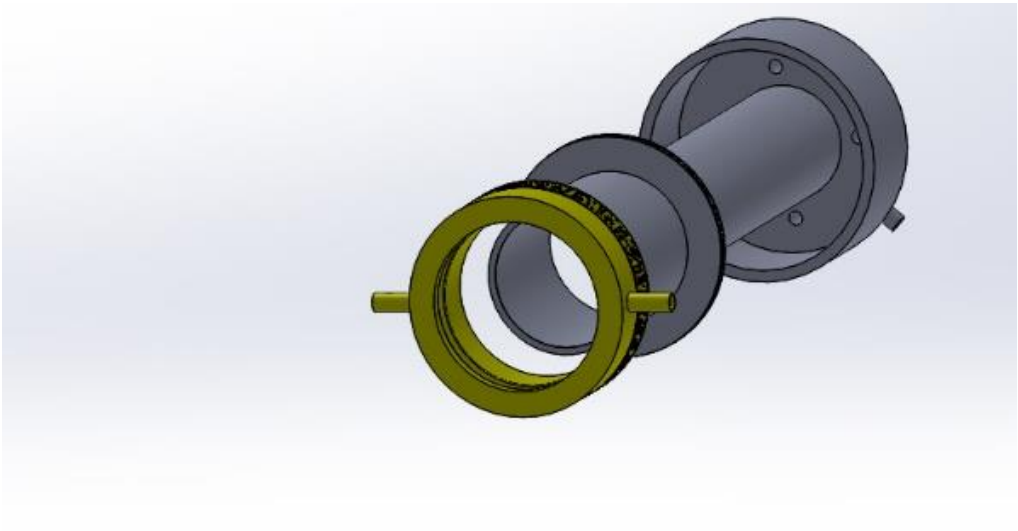

Figure 2.6: Exploded view of the assembled injector.

2.1.2. Drop tube furnace

The DTF comprises an electrically heated coil and a vertical quartz tube with an inner diameter of 6.6 cm and a length of 82.6 cm. It can achieve wall temperatures up to 1200 ºC that are monitored by two thermocouples. The DTF has two opposed rectangular windows, with 2 cm width and 20 cm height, in the heating zone, which is 30 cm long. The temperature profiles inside the DTF were measured using 76 µm diameter R-type thermocouples placed on an appropriate probe. The probe is mounted on a mechanism that allows the thermocouple to move along the central axis of the quartz tube with a positioning accuracy of ±1 mm. Temperature readings were taken from a data acquisition board connected to a computer, being the acquisition time 30 seconds [34].

Figures 2.7, 2.8 and 2.9 show the ambient (air) temperature profile as a function of the vertical distance from the injector along the quartz tube for three DTF wall temperatures – the tip of the injector corresponds to the zero in the horizontal axis. Temperature flutuations can be viewed near the air supply entrance and the injector tip. This happens because the air takes some time to reach the DTF temperature, and due to interactions between the water-cooled injector tip and the hot air.

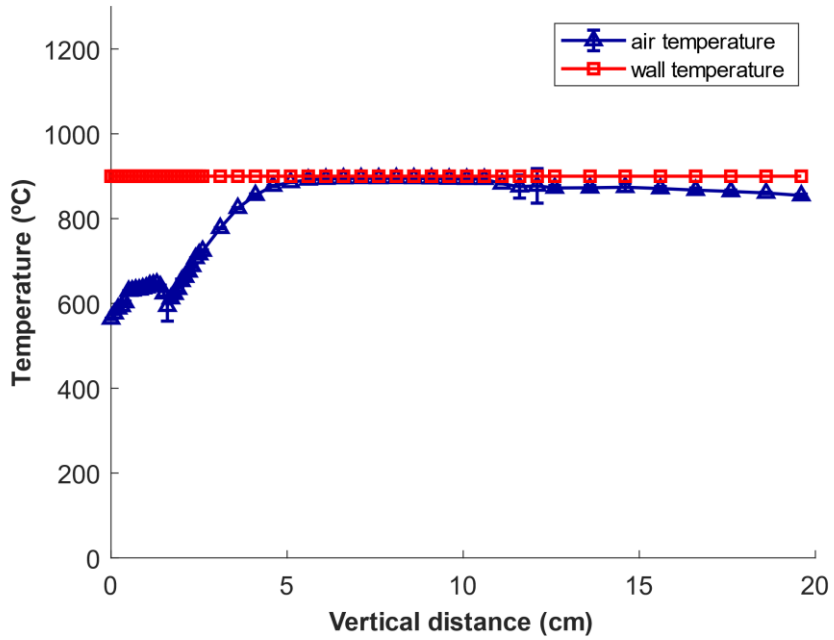

Figure 2.7: Ambient temperature as a function of the vertical distance from the injector tip at 900 ºC.

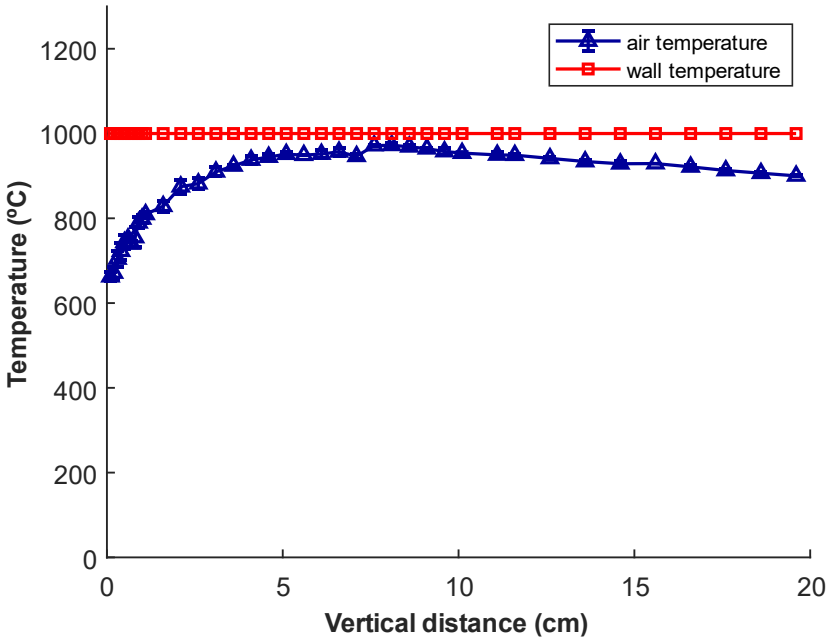

Figure 2.8: Ambient temperature as a function of the vertical distance from the injector tip at 1000 ºC.

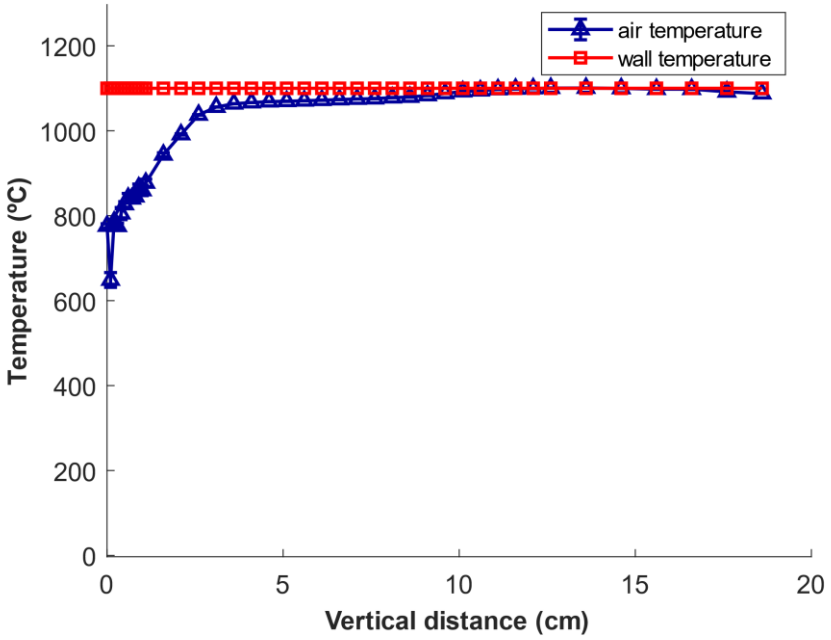

Figure 2.9: Ambient temperature as a function of the vertical distance from the injector tip at 1100 ºC.

2.1.3. Droplet generator system

Figure 2.10 shows a schematic of the droplet generating system.

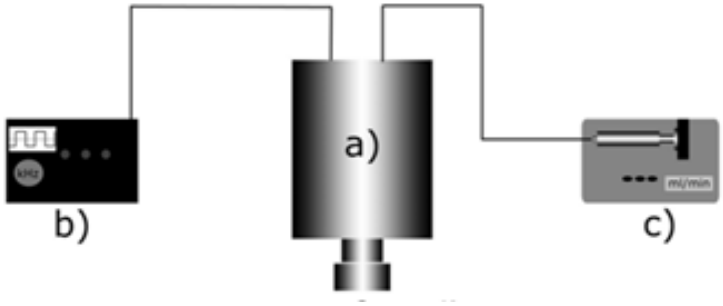

Figure 2.10: Schematic of the droplet generating system [35].

The droplet generator (a) is located on the top of the installation in the injector system, aligned with the DTF and at 50 mm between the axis of the injector and the tip of the injector. The generator was manufactured by TSI and is a Monosize Droplet Generator 100. It produces a stream of uniform size drops in the range of 50 µm to 300 µm, which is a good compromise between actual sizes in practical applications and a good accuracy of the experimental results. Figure 2.11 shows the principle for producing a mono-size droplet stream, where S represents the inter droplet distance, d_d represents the droplet diameter, v_d represents the droplet velocity, and λ_{dis} represents the wavelength of the excitation signal. It relies upon the principle of applying a constant periodic excitation to a laminar liquid jet, which causes surface waves to form and grow as the jet slows down. Breakup into a single droplet per surface wave period thus occurs. This is an established technique of mono-size droplet generation and is commonly used for fundamental droplet studies like vaporization, combustion, levitation, and surface interaction. Droplets were produced with an initial diameter of 155 ± 5 µm, which is an acceptable compromise between actual sizes in practical applications and experimental constraints in order to get good accuracy with the measurements. The mono-size stream of droplets was injected along the axis of the quartz tube, coaxially with the airflow produced by the air supply.

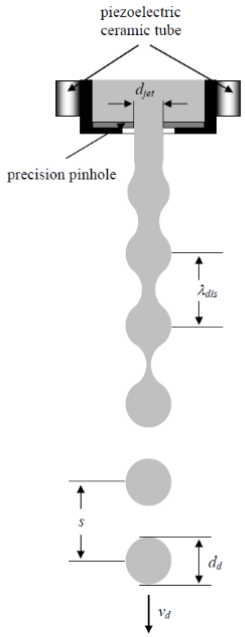

Figure 2.11: Schematic for the method for producing a monosize stream of droplets [35].

Figure 2.12 shows the devices that support the droplet generator, comprising a syringe pump and a signal generator. The excitation frequency was produced by a Fluke PM5136 frequency generator (b), that can produce a square wave with an amplitude of 20 Vpp and a frequency range of 0.1-5 MHz, which fits perfectly in the requirements of the MDG 100.

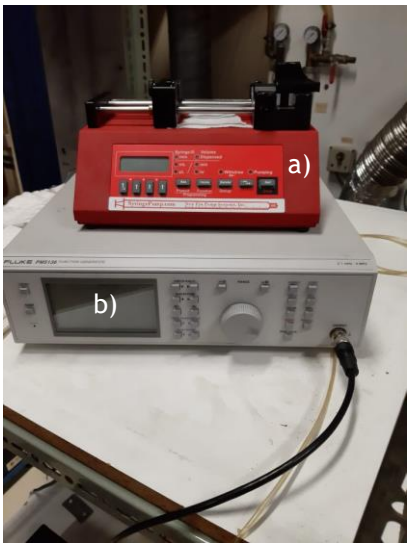

Figure 2.12: Photograph of the a) syringe pump, and b) signal generator.

In order to provide a liquid flow, a syringe pump NE-1000(c) is used, which provided the compatible flow rate with the MDG. A glass syringe was used to ensure that the properties of

the fuel are maintained. It is possible to approximately calculate the droplet diameters using the following relation:

$$D = \frac{6\,Q^{1/3}}{\pi\,f} \quad (2.1)$$

where D is the droplet diameter, Q is the volume flow rate, and f is the excitation frequency.

The diameter of the droplets in micrometers can be represented by:

$$D(\mu m) = 317\,\frac{Q(ml/min)^{1/3}}{f(KHz)} \quad (2.2)$$

In this study, a frequency of 1.5-2.8 kHz , a flow rate of 0.8-1.6 ml/min and two different pinholes with 100 and 200 µm were used. The reason for using different values for flow rate and frequency is because the different fuels present different excitation regimes and different flow properties. With this frequency range it was possible to achieve the required diameter with a staple mono-size stream. The MDG is only capable of producing stable streams with an inter droplet space of 7 droplets, which is not enough to obtain the phenomenon of single droplet ignition. This is due to droplets interact aerodynamically with each other's wake. Consequently, a rotating disk had to be designed in order to increase the inter droplet space, as shown in Figure 2.13. The disc was coupled to an electric motor and a DC power supply that permitted a voltage from 3 V to 12 V. With this power supply it is possible to regulate the rotating disc angular velocity. The disk was placed between the droplet generator and the entrance tip of the injector. This technique has already been applied by other authors [36]. In the beginning, the jet was directed into a recipient until the droplet stream is stabilized. Afterward, the disc was rotated, and the droplets could penetrate the slot for a short time depending on the rotating velocity. With this solution, it was possible to obtain just one droplet per frame and guarantee a single droplet phenomenon.

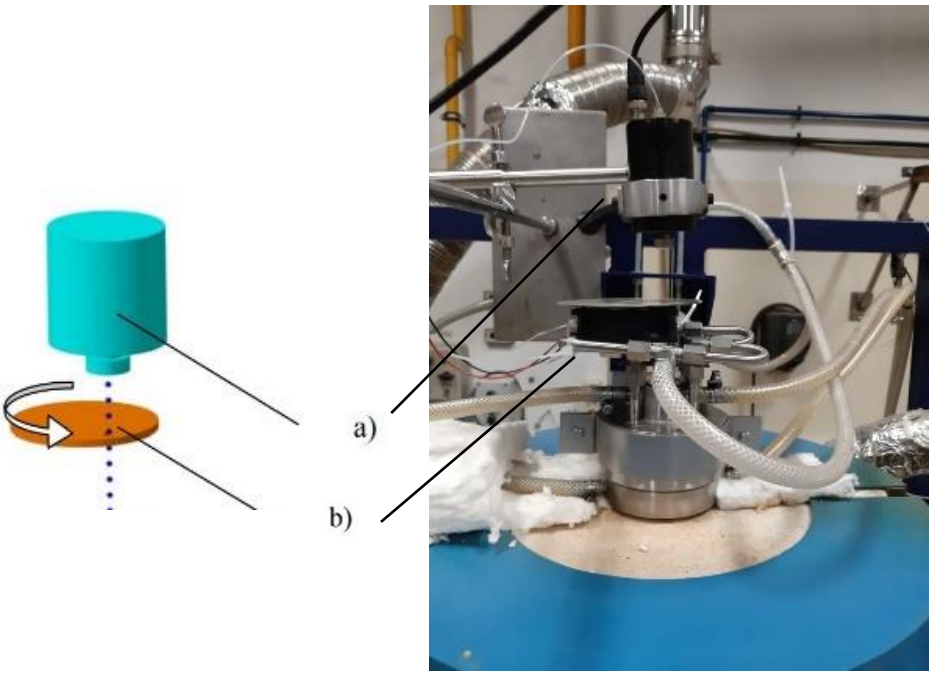

Figure 2.13: Representation of the a) droplet generator, and b) rotating disk.

2.2. Droplet imaging technique and acquisition system

Backlighting imaging is the chosen technique for this work. This method is used for tracking droplet size, position and other kinds of interactions such as droplet impingement. Figure 2.14 shows the typical arrangement of an installation setup using this technique. It consists of the alignment of a light source and an imaging system; then a test object is placed between the lighting and the imaging system. The light source makes the droplet boundaries sharper and ensures that they are easily outlined. As a result, it increases the accuracy of the tracking of droplet size and lifetime. For these reasons, this method has been implemented in a huge number of studies involving droplet characterization. One of the most important factors in the setup is the spatial resolution micron/pixel – the spatial resolution of the image is the ratio of the physical length to image pixels. This is one of the main parameters that affect the accuracy of the results and the size of the image field of view. In order to achieve a high resolution, a microscopic lens must be used. However, this technique only permits tracking the droplet surface boundaries, but not much help for droplet interior tracking.

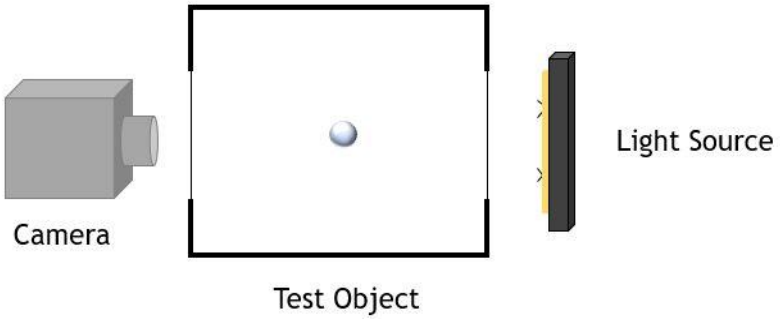

Figure 2.14: Schematic of the backlighting image setup.

Figure 2.14 shows the image acquisition system, which consists of a high-speed camera, a high magnification lens, a homogenous light source and a computer to control the camera and save the images for further image data analysis. The camera used was a CR600x2 from Optronics with a maximum resolution of 1280×1024 at 500 fps and capable of going up to 6000 fps with a resolution of 256×256. During the experiments, a frame rate of 1000 fps was used, which decreased the resolution to 1280×500 and a shutter speed of 8000 s^{-1}. This shutter speed was selected because an increase in its value would mean a reduction in the image brightness. A high magnification lens Zoom 6000® Lens System was attached to the high-speed camera. This is a modular system that permits the magnification of a traditional microscope at a working distance of 300 mm. It is composed of 6.5×Zoom, 12 mm FF, a 0.25× lens attachment and a 2.0× short adapter, with a magnifying range of (0.35-2.25), which makes possible to increase the spatial resolution of the image up to 8.2 μm/pixel. The setup requires background homogeneous illumination to intensify the contrast and to improve the visualization of the images. This illumination was parallel to the droplet falling plane. To provide uniform illumination, a diffusion glass was placed in front of the LED projector. Calibration of the IAS was done before every set of measures with a reference with 76 μm diameter that was placed in the focal plane. Afterward, the scale pixel/mm was determined to allow the treatment of data. This imaging method not only gives information about the droplet size and motion but also about the flame location. Additionally, for each experimental condition, a minimum of 30 single droplets were analyzed.

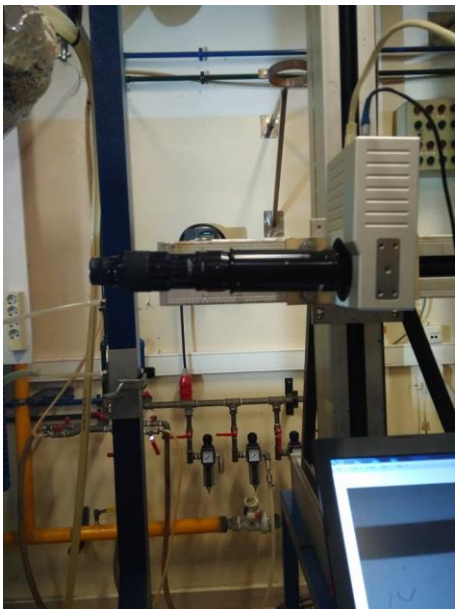

Figure 2.15: Image acquisition system.

2.2.1. Edge detection algorithm

It is necessary to develop a tool that permits to obtain several parameters from the images taken during the experiment such as droplet velocity, signal intensity, droplet area, droplet diameter. Due to this, an edge detection algorithm was used, which enables the acquisition of these parameters.

Under the illumination field, the photographed fuel droplets appear in the recorded image as a darker element. Figure 2.15 shows a sample image of a burning 100% jet fuel droplet and the corresponding background image. There is a sharp transition from light gray to darker gray pixels near the droplet surface, a pronounced gradient of intensity values characterizing the outline region. Near the droplet flame, changes in brightness intensity exist and it is possible to characterize the flame intensity and shape. The properties of each frame are calculated and stored in order to evaluate how this parameter change during evaporation and combustion.

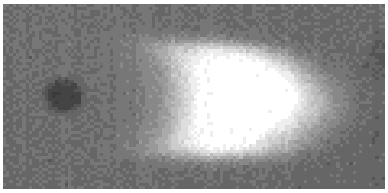

Figure 2.16: 100% JF droplet burning at 1100 ºC.

To determine the drop outline region, it is considered both the brightness difference between the lighter background and the darker droplet and the local brightness gradient. The brightness gradient is determined using four connected pixels in the vertical and horizontal. Both

brightness differences and brightness gradient are calculated for each pixel in each image containing a droplet. The analysis indicates that a well defined threshold value of brightness difference coinciding with the peak gradient of brightness, presumably marking the drop surface. Before each analysis, a region of interest (ROI) involving the droplet and its flame was selected. This simplifies the process it greatly reduces the area that the algorithm as to process. Due to loss of precision at lower diameters, two methods of calculating the droplet diameter were used. The first method was to calculate the brightness difference between the droplet and its background for each pixel within the ROI and mark the droplet area of pixels with a defined threshold based in brightness intensity as described above. After the droplet area is well defined, its mean diameter is calculated using an ellipse coincident with the droplet surface. Figure 2.16 shows an example of the edge detection method. Later in the droplet lifetime, the droplet reaches a reduced diameter and the uncertainties become too large to measure its diameter with precision. From beyond this point $(\frac{D^2}{{D_0}^2}) = 0.2$, it's necessary to use other types of analysis. So linear regression is used for these later stages, with the first point being the last instant where droplet diameter was measured with precision and the last point when the droplet is completely fully evaporated.

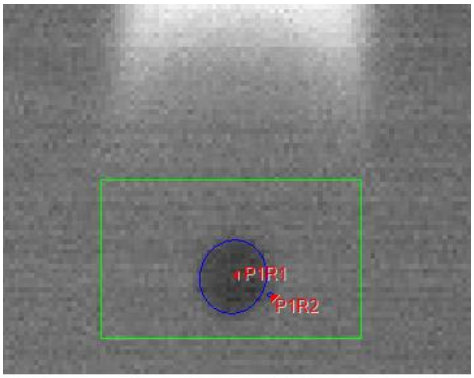

Figure 2.17: Edge detection example.

2.2.2. Ignition criteria

The ignition criterion used in this work is based on visible light, similarly to what was done by other authors [37, 38]. This technique is relatively simple to implement because the visible light signal intensity is easy to capture with the IAS. Although soot is included in the visible light signal this method has proved to be a good indicator of ignition [39]. In this work, ignition was considered to occur when 15% of the maximum pixel luminosity was reached – these criteria have already been used in earlier works [37]. The light intensity signal of the images was normalized by the maximum luminosity intensity of each video since droplets exhibit different ratios of maximum luminosity to the baseline luminosity. The code reads the data from the .tiff files, stores it in matrices, eliminates the background noise, and identifies the frame in which the pixel value was closest to 15% of the maximum luminosity intensity.

2.3. Fuel characterization

In this section, properties of both fuels and its mixtures (75% JF - 25%HVO, 50% JF - 50% HVO, 25% JF – 75% HVO) are present and discussed. Table 2.1 shows the properties of the conventional, alternative fuel and their blends, the fuel properties were measured in IST [40]. Some of the blend's properties can be calculated with the knowledge of the properties of the two blending components. The values of other parameters need to be measured, for example, the cetane number and viscosity. The mixtures were prepared with the aid of a volumetric pipette, with a capacity of 50 ml ± 0,05 ml. Afterward, they were stored in a glass recipient due to its reactive tendency with polymers (rubbers). This way the fuel properties are preserved.

From the point of view of atomization, the most important properties are density, surface tension, and viscosity. In addition, from the point of view of combustion the more relevant properties are heating value, the ultimate analysis, metal content, flash point, freezing point, cetane number, and auto-ignition point.

Table 2.1: Fuel properties [40].

	100%JF	75%JF	50%JF	25%JF	0%JF	Value	Norm
Acidity [mgKOH/g]	0.001	-	0.003	-	0.005	≤0.10 ≤0.015	D1655 D7566_A2
Sulfur [%w]	0.09	0.07	0.045	0.02	<0.0001	≤0.30 ≤0.015	D1655 D7566_A2
Aromatics [%w]	13.8	10.4	7.0-	3.5	0.2	≤26.5 ≥8.4	D7566_A2
E.condutivity [pS/m]	335	-	-	-	206	50-600	D1655
Flashpoint [°C]	38.5	-	-	-	77	≥38 ≥38	D1655 D7566_A2
Surface tension [mN/m]	25.37	-	24.64	-	26.6		
Density [kg/m³]	785.8	783.9	782.0	779.9	778.2	775-840 730-770	D1655 D7566_A2
Freezing point [°C]	-67	-	-	-	-30.4	≤-47 ≤-40	D1655 D7566_A2
Viscosity -20°C 40°C [mm²/s]	1.4	-	-	-	2.93	≤8.0	D1655
LHV [MJ/kg]	43.34		43.60		43.86	≥42.8	D1655
HHV [MJ/kg]	46.02		46.53		47.05		

2.3.1. Density

Density is defined as the ratio between the mass and the volume of a homogeneous object/solution at a specific temperature. This parameter is very important because the AJF and the jet fuel need to have a similar density in order to promote a good performance of the engine and to be able to serve as a "drop-in" fuel. This analysis has been done in previous works [40].

As can be seen in Table 2.1, the density decreases while the percentage of jet fuel decreases. The jet-fuel exhibits the higher value but the difference between the different fluids are relatively small, which means that the density value of mixtures fit perfectly within the current legislation D1655 (775-840 kg/m^3).

2.3.2. Viscosity

Viscosity is a measure of how resistant a liquid is to flow. Kinematic viscosity is an important property of biodiesel since it affects the operation of fuel injection equipment, particularly at low temperatures when an increase in viscosity affects the fluidity of the fuel. Moreover, high viscosity may lead to the formation of soot and engine deposits because of insufficient atomization. These properties must be considered because blends will be affected by the addition of the AJF and it will affect atomization, which is critical in an injection system [41].

2.3.3. Surface tension

The surface tension is defined as the specific free energy of a liquid surface at the interface with another fluid according to the specifications. Surface tension is one of the principal factors that affect atomization making it very important in phenomena as spray combustion, due to this, the values need to be accordingly with the legislation to ensure optimal performance. However, considering the small variation of this physical property in the three fluids used in the experiments, the surface tension can be considered as almost constant. Therefore, it will be expected that the surface tension will not have a crucial role in the variation of the outcomes [41].

2.3.4. Cetane number

The Cetane number is a measure of a fuel's ignition delay, the time period between the start of injection and the first identifiable pressure increase during the combustion of the fuel. In a diesel engine, higher cetane fuels will have shorter ignition delay periods than lower cetane fuels.

2.3.5. Sulfur content

Sulfur can occur in both gaseous and liquid fuels. In gas fuels, it is usually present as hydrogen sulfide (H_2S). Liquid fuels, especially heavy fuel oils, can contain very high levels of sulfur; however, new legislations are driving operators to use low sulfur diesel or fuel oils. Hydrogen sulfide is highly toxic and can pose unique challenges to operators as well as in the operation of gas turbines. Besides specific health and safety requirements, H_2S (also sulfur in liquid fuels) can combust producing SOx (SO_2/SO_3) emissions to the atmosphere, which reacts in the presence of moisture resulting in weak acid production (acid rain). Where SOx legislation exists, treatment of the fuel at source to remove or lower H_2S (or sulfur in liquid fuels) is necessary [21]. The blending of HVO in JF decreases the sulfur content, which supports the potential of biofuels due to a reduced content in fuel pollutants and help to reduce emissions.

2.3.6. Flash point

The flash point (FP) of a fuel is the temperature at which it will ignite when exposed to a flame or spark, i.e., it is the lowest temperature at which fuel emits enough vapors to ignite. The FP varies inversely with the fuel's volatility. HVO presents a larger value for flashpoint, which indicates that it is less volatile and less reactive comparatively to JF. This difference can affect the burning efficiency and the stability in the combustion chamber.

2.3.7. Jet-A1

Jet-A1 is a fuel specially designed for gas turbine applications in the aeronautical industry. Due to this, jet fuel is used as a reference in this work. Jet-A1 is a fossil fuel constituted by several components, with several carbons comprehend between 8 and 16 in its molecular chains. 70% to 85% of the fuel is made up of paraffins, with normal straight-chain, branched chain isoparaffins and cycloparaffins or naphthenes being present. The exact split between normal, iso and cyclic is variable and depends on the raw crude used in the refinement process [7]. The aromatics are present at less than 25% and are unsaturated cyclic hydrocarbons containing one or more six carbon ring structures. Since there are deficient in hydrogen, they have high heat content per unit volume but lower heat content per unit mass compared to paraffins with the same carbon number. This wide variation in compounds found in jet fuel causes the combustion engineer difficulties when trying to model any combustion process. Finally, all known crudes contain sulfur in varying amounts. The total sulfur content is currently limited to 3000 ppm by the legislation.

2.3.8. NExBTL

The fuel used in this work is an HVO, known by the commercial name of NExBTL. It is a biofuel used for land application in diesel engines, but its properties are very similar to aviation fuel.

This fuel presents a very similar density in comparison with jet-A1 and it is composed of straight chain and branched paraffins the simplest type of hydrocarbon. NExBTL is a mixture of straight chain and branched paraffins the simplest type of hydrocarbon molecules from the point of view of clean and complete combustion. Typical carbon numbers are (C15-C18). Paraffins exist also in fossil diesel fuels which additionally contain significant amounts of aromatics and naphthenic. Aromatics are not favorable for clean combustion. HVO is practically free of aromatics and its composition is quite like GTL and BTL diesel fuels made by Fischer-Tropsch synthesis from natural gas and gasified biomass. This fuel is practically free of metals and ash-forming elements and sulfur-free which leads to the need for adding additives to improve lubricity. HVO belongs to the group of hydrocarbons which are miscible with a hydrocarbon matrix of a fuel blend. Therefore, the use of HVO as a blending component does not need to be regulated further through technical standards. In addition, the NExBTL behaves like a fossil fuel in terms of operating logistics because of its stability (no need for "use before" date) and doesn't raise issues with water separation, microbiological growth, and impurities causing precipitation above cloud point [43].

Japan airlines have also demonstrated the feedstock independence of hydroprocessed jet fuel through incident free operating of one of its Boeing 747-300 aircraft out of Tokyo. The roundtrip test flight, which departed on January 2009, operated one of four engines on a 50/50 blend of conventional jet fuel and hydro processed biomass feedstock, consisting of Camelina (42%), Jatropha (8%) and Algae (<0.5%). The success of the recent test campaigns has not only highlighted gas turbine biomass product compatibility but also demonstrates the technological readiness and feedstock independence of the hydrotreatment process. However, only blended with jet fuel, can meet the requirements for use in the aeronautical sector described in ASTM D1655 E D7566 [30, 33] Therefore, a 50% blending ratio between the biofuel and the JF was chosen for the flights. This ratio represents a feasible initial target for future approvals within the existing specifications [6].

Chapter 3

3. Results and discussion

This chapter presents and discusses the experimental results. Firstly, the conditions under which the tests were conducted are given, then the results on the visualization of burning droplets and on disruptive burning are presented, and, finally, the droplet size evolution and burning rate are reported.

3.1. Droplet characterization

For single droplet ignition, it is very important to have knowledge about the operating conditions and the factors that affect the droplet size evolution. The Reynolds number is an important dimensionless number because it permits to characterize the flow regime. The air properties were taken from the ISA (International standard atmosphere) and the droplet velocity and diameter were measured using the image acquisition system (IAS). In order to calculate the droplet average velocity relative to the gases, the mean condition of the airflow in the quartz tube must be known. Consequently, the mean flow velocity must be calculated for each condition. Table 3.1 shows the air properties for each condition. The pressure inside the DTF is the ambient pressure and the air density was calculated using:

$$\rho = \frac{p}{Rd \times T} \qquad (3.1)$$

where Rd is the specific gas constant for dry air – Rd = 287.058 J/(kgK). The dynamic viscosity was calculated using the Sutherland law:

$$\mu = \mu_{ref} \left(\frac{T}{T_{ref}}\right)^{\frac{3}{2}} \left(\frac{T_{ref} + s}{T + S}\right) \qquad (3.2)$$

where μ is the dynamic viscosity (μ_{ref} = 1.716 x 10^{-5} kg/(ms)), T is air temperature (T_{ref} = 273.11 K), and s is the Sutherland constant (s = 110.56 K). With the air properties, it is possible to calculate the mean air velocity and Reynolds number (the characteristic linear dimension used was the hydraulic diameter) inside the quartz tube for each condition, with the respective values shown in Table 3.2. Table 3.2 shows that the Reynolds number in the quartz tube is relatively low, meaning it should have a low turbulent intensity and provide a good stable test atmosphere. Droplets entered the quartz tube with a nearly constant velocity of approximately 0.6 m/s. Figure 3.1 shows the velocity profile relative to the gas for the droplets entering the

quartz tube. Thus, it is possible to calculate their mean droplet Reynolds number (Re_D) through the air properties, droplet diameter, and velocity.

Convection significantly affects the burning characteristics (flame location and minimum temperature for ignition) and the burning rate, making the droplet velocity profile and Reynolds number is essential to fully characterize the phenomenon. Figure 3.2 shows the droplet Reynolds number as a function of the normalized diameter. From $(\frac{D^2}{{D_0}^2}) = 0.1$, it is not possible to determine the droplet velocity and, consequently, the droplet Reynolds number. It is seen that the droplet Reynolds number reduces as its diameter reduces. Additionally, droplets have a higher deacceleration at the lower diameters because droplets are injected with moderate velocity and, as droplet loose mass, the diffusive forces overcome the inertial forces. So, diffusive forces are felt with more intensity at lower diameters.

Table 3.1: Air density for each operating condition.

	900 ºC	1000 ºC	1100 ºC
Air density ($\frac{kg}{m^3}$)	0.30	0.27	0.25
Dinamic viscosity ($Pa.s$)	45.6 x 10^{-6}	47.88 x 10^{-6}	50.01 x 10^{-6}

Table 3.2: Flow properties for each condition.

	Airflow velocity (m/s)	Re	Re_D
900 ºC	0.11	47.0	0.6
1000 ºC	0.12	44.8	0.5
1100 ºC	0.12	42.8	0.4

The instabilities in droplet velocity affect the burning rates and are responsible for fluctuations in the burning constants. It is not possible to quantify the magnitude of the effect because the burning constant depends on a large range of parameters. From this analysis, it can be seen that as the temperature increases, the Reynolds number reduces. The reduction is due to variations in the air properties (dynamic viscosity and density) caused by the temperature increase.

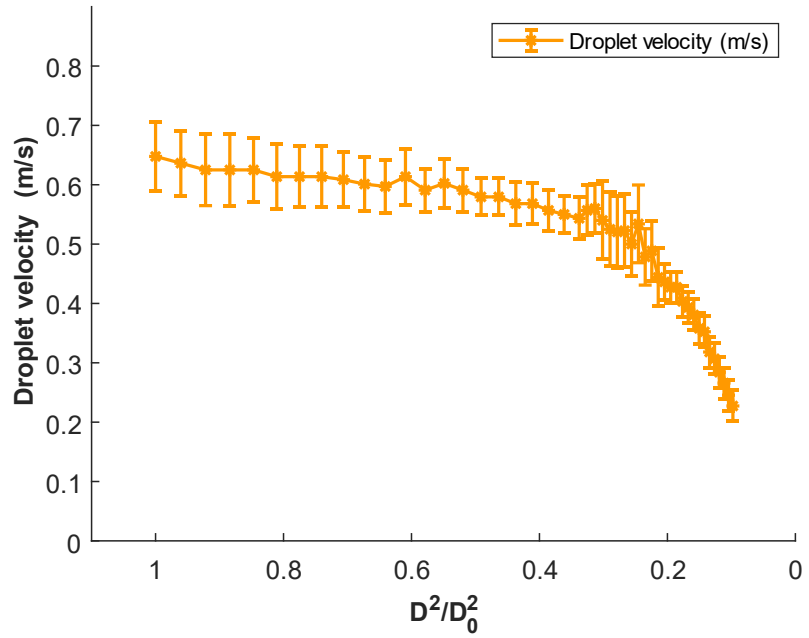

Figure 3.1: Droplet velocity as a function of the normalized diameter.

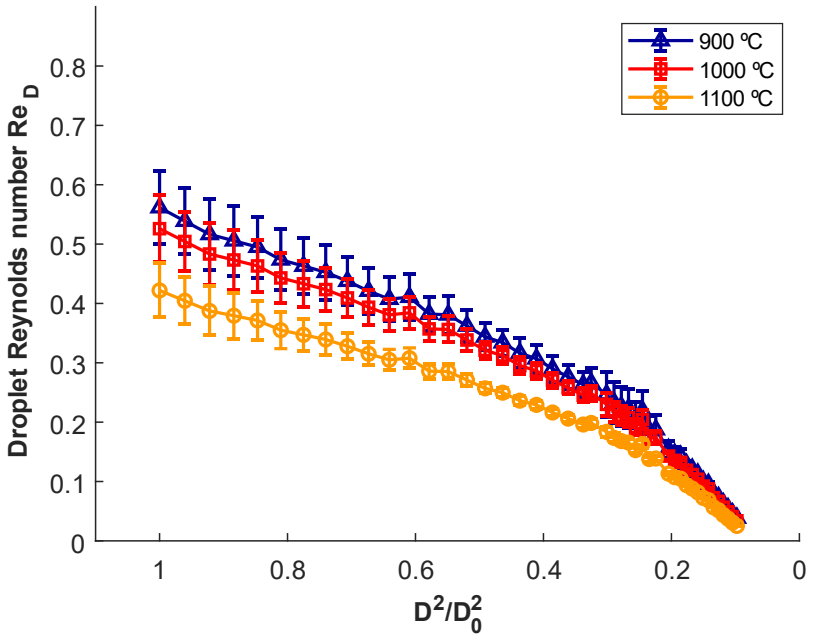

Figure 3.2: Droplet Reynolds number as a function of the normalized diameter.

3.2. Visualization of the single droplet combustion

Figure 3.3 shows sequences of instantaneous images of burning droplets at different temperatures. After injection into the quartz tube, the droplets ignite due to the high air temperature and a flame is established at the wake of each droplet, as seen in Fig. 3.3. The figure also reveals that the flame intensity (luminosity) decreases and the droplet lifetime increases as the ambient air temperature decrease from 1100 ºC (Fig. 3.3a) to 900 ºC (Fig. 3.3c), regardless of the composition of the fuel mixture. The composition of the fuel mixture also affects the burning characteristics mainly due to the different content of aromatics in the different fuel mixtures. In particular, the flame intensity increases, and the flame root moves closer to the droplet as the percentage of jet-A1 in the fuel mixture increases. Interestingly, it was observed the occurrence of disruptive burning for the fuel mixture with 75% of jet-A1 (Fig. 3.3a). At t = 16 ms (Fig. 3.3a) a sudden increase in the flame size and intensity occurs. This phenomenon, often called puffing, is characterized by the release of volatiles due to the breakup of an expanding gas bubble formed inside the fuel droplet. This event is followed by a rapid decrease in the diameter of the droplet, as seen at t = 24 ms. These observations are consistent with other studies [12]. The occurrence of puffing precedes the appearance of micro-explosions (M-E), as observed at t = 40 ms, with the establishment of a spherical flame, and no visible droplet. The event of micro-explosions reduces significantly the droplet lifetime. It is evidenced that disruptive burning processes occur in a very short time interval, such as the micro explosion, that is stated to occur in less than 200 μs [19]. This suggests that the imaging rate should be higher than 5000 frames per second for the proper tracking of every step of the phenomena. Therefore, at the frame rate used in these experiments, it is not possible to observe in detail every step of the M-E and “puffing” [19].

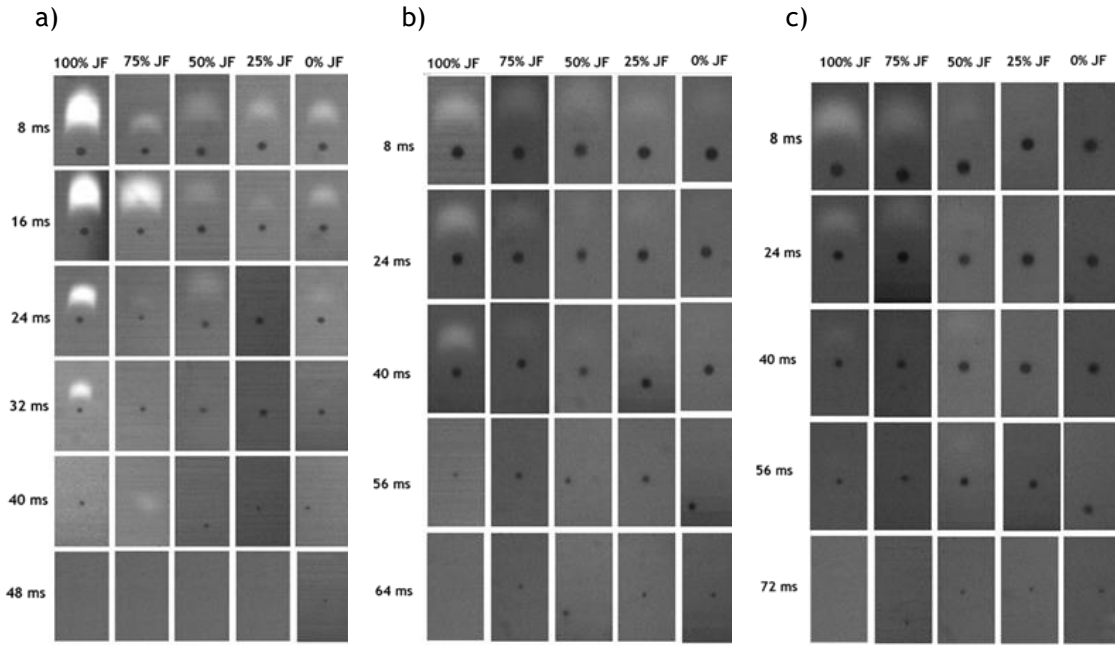

Figure 3.3: Sequences of instantaneous images of burning droplets at different temperatures: a) 1100 ºC; b) 1000 ºC; c) 900 ºC.

3.3. Occurrence of micro explosions

In this section, the discussion of the phenomenon of micro explosions is addressed in a more detailed analysis. M-E is a highly unstable phenomenon and it is not possible to accurately predict when it occurs. Figure 3.4 shows the occurrence percentage of micro explosion for the mixture 75% JF. As referred earlier, a minimum of 30 single droplets were analyzed for each experimental condition. It is possible to see that the phenomenon doesn't occur for every droplet, which might be due to the high puffing intensity and the main gas bubbles have already broken up, or due too small differences in the emulsion of the blending agents inside the droplet. However, a relatively high percentage of micro explosions occur (71% of the total droplets). Figure 3.4 shows the occurrence of micro explosions for a range of droplet diameters. The incidence of micro explosion occurred between 55 and 70 μm suggests that this range of diameter favors disruptive burning. From a global perspective, however, the range of diameters for the occurrence of M-E is relatively small, with a global variation of 15 μm. This is a relatively small value taking into account the unstable nature of the phenomenon. This highlights the potential of controllable disruptive burning in engineering applications because M-E highly enhances the secondary atomization and reduces droplet lifetime and, thus, improves the burning properties [44].

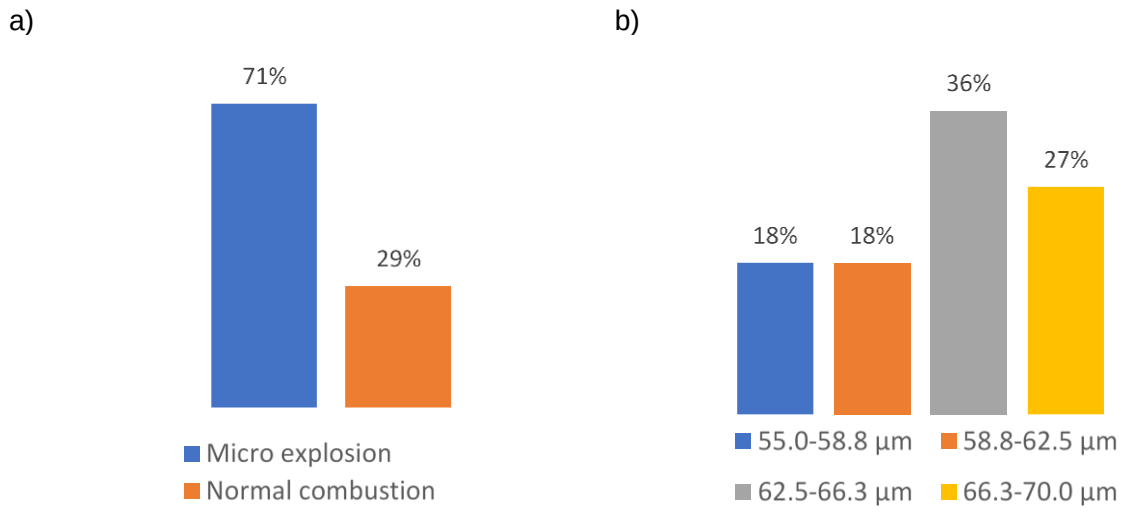

Figure 3.4: Characterization of the micro-explosions for the fuel mixture with 75% of jet-A1 at 1100 ºC: a) Frequency of micro-explosions; b) droplet diameter at the micro-explosion instant.

3.4. Droplet size evolution and burning rate

As stated earlier, tests were performed for three different temperature conditions (900, 1000, 1100 ºC) and the 5 different blends referred to earlier. The analysis below is based on the well known D^2 law. Figures 3.6, 3.7 and 3.8 show the normalized droplet diameter as a function of the normalized time for the three different temperatures studied. It is seen that the results are in good agreement with the D^2 law, which predicts that the normalized square diameter decreases linearly with the time with a nearly constant slope, the so called droplet burning rate, K_b . In this analisys it is assumed that the droplet burning rate K_b is equal to the droplet evaporation rate K. The normalization process is done by dividing both the squared diameter and the time by the initial squared droplet diameter ($D_0{}^2$). Figure 3.5 shows the normalized droplet diameter as a function of the normalized time for 100% JF at three different temperatures. JF is a highly multi-component fuel with a variable composition, so its burning rate variations can also be dependent on fuel composition evolution. However, the results are in good agreement with the "D^2 law" even in presence of forced convection.

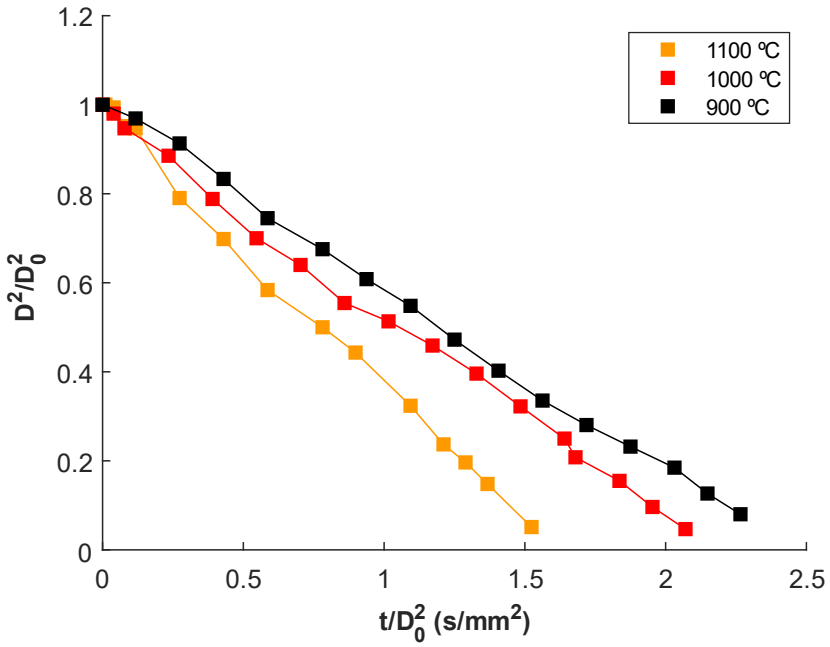

Figure 3.5: Normalized 100% JF droplet diameter as a function of the normalized time at different temperatures.

Moreover, the evolution of the normalized droplet diameter is quite similar for all conditions, except for the fuel mixture with 75% of jet-A1 at 1100 ºC (Figure 3.6). The droplets of pure HVO present the longest burning time and the droplets of pure jet-A1 the shortest one. The evolution of the droplets of the fuel mixture with 75% of jet-A1 presents the most distinctive behavior because of the occurrence of puffing and micro explosions, as discussed earlier. Finally, Figures 3.6, 3.7 and 3.8 reveal that the droplet burning time increases as the air temperature decreases.

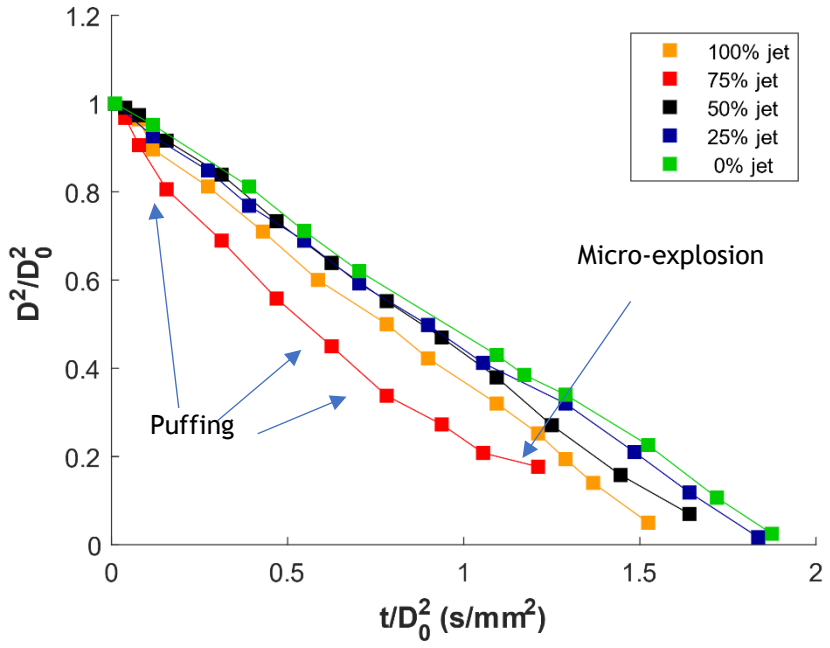

Figure 3.6: Normalized droplet diameter as a function of the normalized time at 1100 ºC.

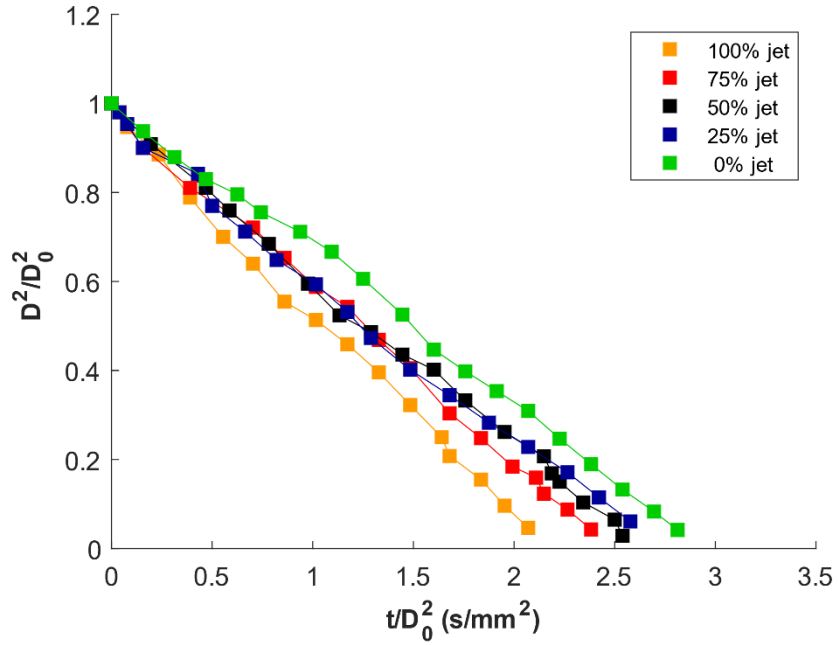

Figure 3.7: Normalized droplet diameter as a function of the normalized time at 1000 ºC.

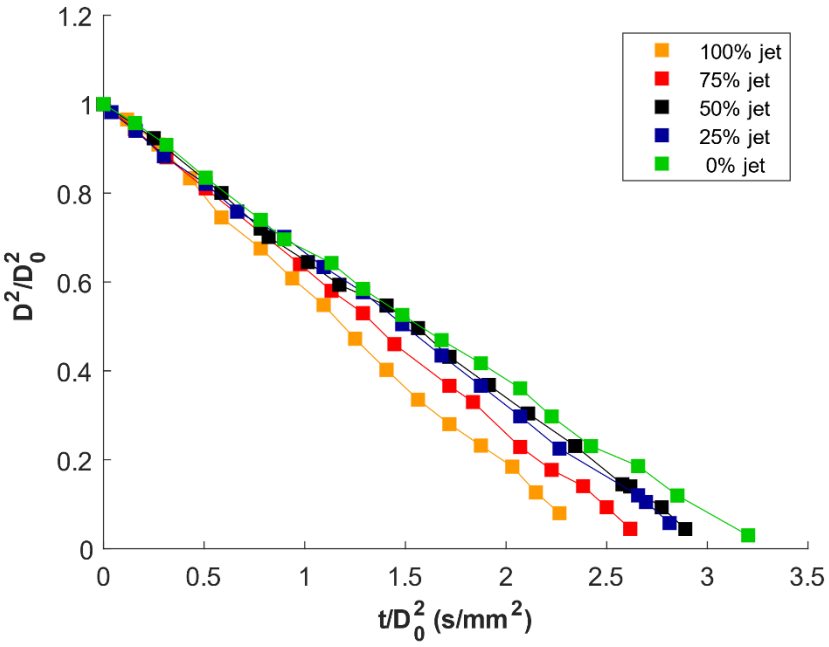

Figure 3.8: Normalized droplet diameter as a function of the normalized time at 900 ºC.

To obtain further insight into the behavior of burning droplets, the burning rates were calculated for each blend in different conditions. Figures 3.9, 3.10 and 3.11 show the burning rate as a function of the normalized time at different temperatures. The burning rates were calculated from the data presented in Figures 3.6, 3.7 and 3.8 following the procedures described in [45]. More specifically, the burning rate, $K_b = -\mathrm{d}\left(\frac{D^2}{\mathrm{dt}}\right)$ was calculated through the derivation of the D^2 curves. This method raises a problem because derivation greatly increases any experimental uncertainties, so a three-point moving average was employed in both the burning rate graphics and in the D^2 evolutions to smoothen the curves. This curve presents a clear unsteady behavior, even though the D^2 curves present a strong linear tendency. With the exception of the fuel mixture with 75% of jet-A1 at 1100 ºC (Figure. 3.9), all droplets present a similar burning behavior, with an initial rapid increase in the burning rate, followed by an almost constant evolution of it until the end of the droplet lifetime. The droplets with 75% of jet-A1 jet present a distinct behavior due to the occurrence of puffing and micro explosions, discussed earlier, that enhances K_b. Later, in the 75% jet-A1 D^2 curve, a reduction in the slope occurs at the later stages before the occurrence of micro explosions due to the small expansions that the droplets suffer before the breakup. These expansions occur due to the expansion of inner gas bubbles that nucleate inside the fuel droplet [46]. It can also be concluded that fuels with higher aromatic contents (cf. Table 1) tend to have higher burning rates.

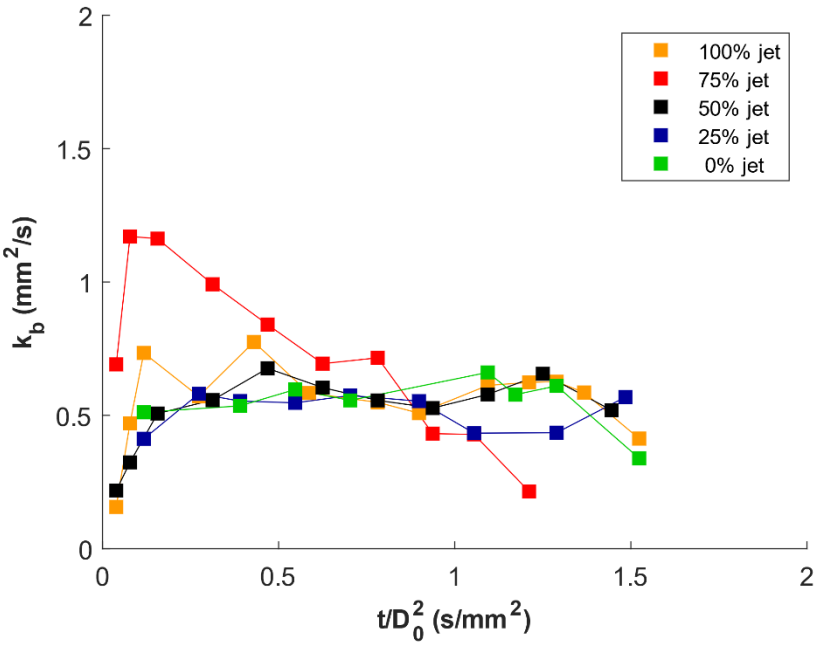

Figure 3.9: Droplet burning rate as a function of the normalized time at 1100 ºC.

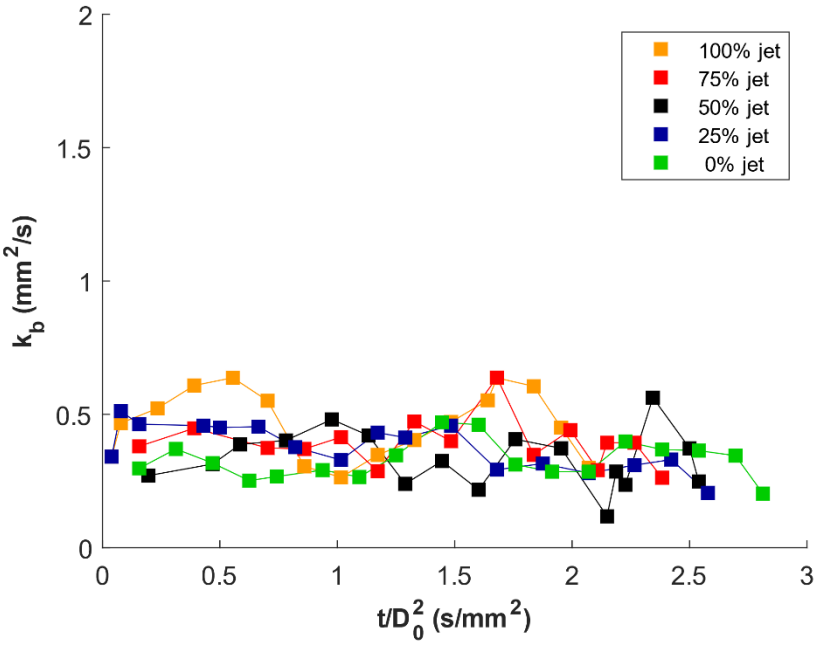

Figure 3.10: Droplet burning rate as a function of the normalized time at 1000 ºC.

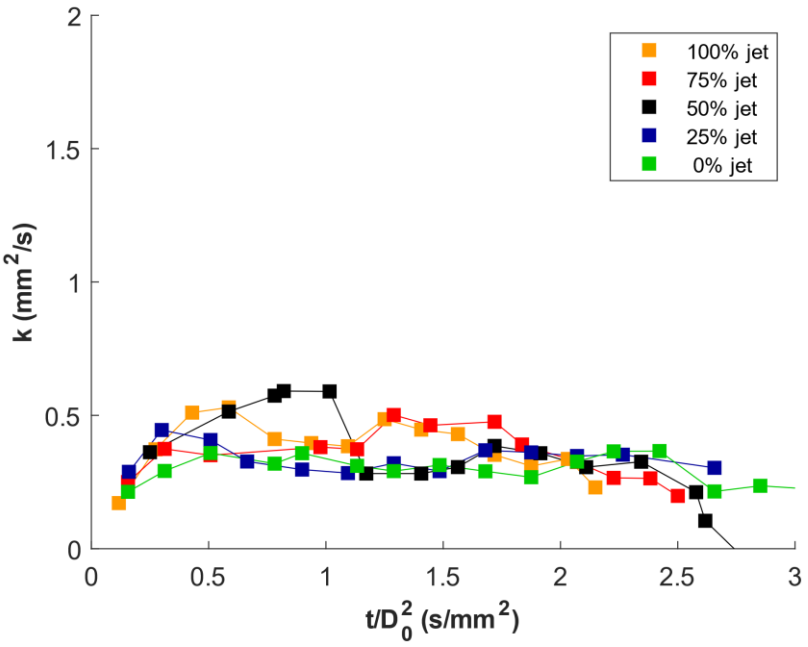

Figure 3.11: Droplet burning rate as a function of the normalized time at 900 °C.

Figure 3.12 shows the global burning rates as a function of the air temperature, and their values can be seen in detail in table 3.3. Despite some unsteadiness in the curve, their temporal variations during the quasi-steady period can be small enough to extract a global burning rate for each fuel and condition, thus extracting the average burning rate. These global burning rates are obtained by fitting the quasi-steady segments of the D^2-t curves to lines by least-squares best-fit. The quasi-steady segment was arbitrarily defined as the interval from $(\frac{D^2}{{D_0}^2})$ = 0.9 to $(\frac{D^2}{{D_0}^2})$ = 0.2, excluding therefore initial transient heating and later stages in droplet lifetime where the uncertainties become the order of magnitude of the size of the droplet. By doing this, a global burning rate was extracted for each test condition and each mixture. This way, global effects can be compared between conditions and conclude that an increase in the ambient temperature leads to an increase in the burning rate. Also, it is seen that as the jet-A1 increases in the fuel mixture, the burning rate also tends to increase. The exception to this behavior occurs for the air temperature of 1100 °C, where the highest burning rate happens for the droplets with 75% of jet-A1. When comparing the data for the three air temperatures, it is observed that the differences between the global burning rates of different fuels tend to be smaller at 1100 °C. This can be attributed to differences in the volatility of each mixture, which tends to be larger at lower temperatures. The effect can also be noted through an earlier flame extinction in the mixtures with less percentage of jet fuel, leading to the conclusion that the composition of the mixtures greatly affects the flame characteristics, this aspect was addressed in detail in the previous section.

Table 3.3: Global burning rate.

$K\ (\frac{mm^2}{s})$	100%JF	75%JF	50%JF	25%JF	0%JF
1100°C	0.62	0.67	0.59	0.54	0.52
1000°C	0.46	0.41	0.37	0.36	0.34
900°C	0.41	0.37	0.34	0.33	0.3

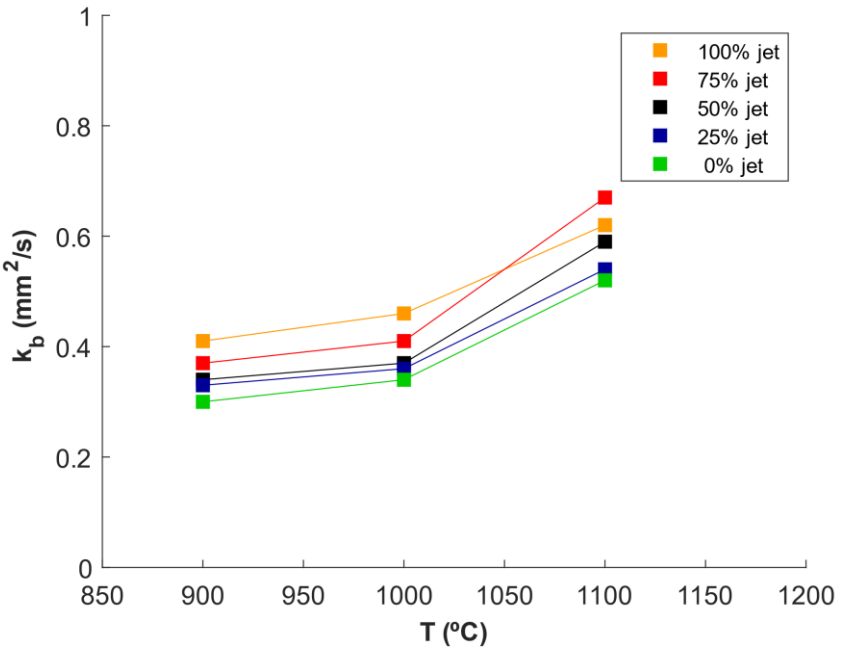

Figure 3.12: Global burning rates as a function of the temperature.

Chapter 4

4. Closure

In the first section of this chapter, the relevant conclusions are presented. Then, the second section is dedicated to future work, where several suggestions are proposed to improve the knowledge regarding this theme.

4.1. Conclusions

The main conclusions from this work are as follows:

1. After ignition, a flame is established at the wake of each droplet for all test conditions. Flame intensity decreases and the droplet lifetime increases as the air temperature decreases, regardless of the composition of the fuel mixture. As the percentage of jet-A1 in the fuel mixture increases, the flame intensity increases, and the flame root moves closer to the droplet.
2. The occurrence of puffing followed by micro explosions was observed for the fuel mixture with 75% of jet-A1. This phenomena enhanced the secondary atomization and reduced significantly the droplet lifetime.
3. The droplet diameters follow the D^2 law, being quite similar for all conditions, except for the fuel mixture with 75% of jet-A1 at 1100 ºC. The droplets of pure HVO present the longest burning time and the droplets of pure jet-A1 the shortest one. The droplet burning time increases as the air temperature decreases.
4. An increase in air temperature leads to an increase in the global burning rate. As the amount of jet-A1 increases in the fuel mixture, the burning rate also tends to increase.

4.2. Future work

The first suggestion is to investigate the effect of the forced convection in the burning characteristics of single droplets constituted from a blend of two fuels. Forced convection highly affects the emulsion of the fuels and this parameter is crucial to the understanding of the disruptive burning phenomena.

Another suggestion is to study the diameter droplet evolution in different oxygen concentrations and evaluate how the different mixtures are affected by the different ambient conditions.

It should be noted that studies of multi-component fuels should be aimed at spray atomization. Further studies should focus on spray combustion and the influence of the biofuel in the burning characteristics and in the emission of pollutants.

Finally, a study regarding the controllability of micro explosions in sprays might be an interesting area of study and an important step for further improving the secondary atomization.

5. References

[1] International Air Transport Association, *IATA Sustainable Aviation Fuel Roadmap,* International Air Transport Association, 2015.

[2] Airbus, *Global networks global citziens*, Airbus Market forcast 2018-2038, 2018.

[3] C. Scherer, *Airbus Global Market Forcast 2019-2038*, Airbus Market forcast 2019-2039, 2019.

[4] R. Parker, M. Lathoud, "Green aero-engines: Technology to mitigate aviation impact on environment*", Proceedings of the Institution of Mechanical Engineers, Part C: Journal of Mechanical Engineering Science*, vol. 224, no. 3, pp. 529–538, 2010.

[5] I. Kubičková, D. Kubička, "Utilization of triglycerides and related feedstocks for production of clean hydrocarbon fuels and petrochemicals: A review", *Waste and Biomass Valorization*, vol. 1, no. 3, pp. 293–308, 2010.

[6] T. Rahmes, J. Kinder, "Sustainable Bio-Derived Synthetic Paraffinic Kerosene (Bio-SPK) Jet Fuel Flights and Engine Tests Program Results", 9th AIAA Aviation Technology, Integration, and Operations Conference (ATIO), 2009.

[7] S. Blakey, L. Rye, C. W. Wilson, "Aviation gas turbine alternative fuels: A review", *Proceedings of the Combustion Institute*, vol. 33, no. 2, pp. 2863–2885, 2011.

[8] IPCC, *Climate Change 2007: Synthesis Report,* Intergovernmental Panel on Climate Change, 2007.

[9] D. Lee, D. Fahey, P. Forster , "Aviation and global climate change in the 21st century", *Atmospheric Environment*, vol. 43, no. 22–23, pp. 3520–3537, 2009.

[10] IPCC, *Aviation and the global atmosphere*, Ipcc special report, 1999.

[11] M. Birouk, I. Gökalp, "Current status of droplet evaporation in turbulent flows", *Progress in Energy and Combustion Science*, vol. 32, no. 4, pp. 408–423, 2006.

[12] G. Godsave, "Studies of the combustion of drops in a fuel spray", Symposium (International) on Combustion, vol. 4, no. 1, pp. 818–830, 1953.

[13] D. B. Spalding, "Combustion liquid fuels", Symposium (International) on Combustion, Vol. 4, no. 1, pp. 847-864, 1953.

[14] P. Coelho and M. Costa, *Combustão,* Edições Orion, 1st edition, 2007.

[15] I. Awasthi, D. N. Pope, G. Gogos, "Effects of the ambient temperature and initial diameter in droplet combustion", *Combustion and Flame*, vol. 161, no. 7, pp. 1883–1899, 2014.

[16] H. Ghassemi, S. Baek, "Experimental study on evaporation of kerosene droplets at elevated pressures and temperatures", *Combustion Science and Technology*, vol. 178 , no.9, pp. 1669-1684, 2006.

[17] T. Saitoh, S. Ishiguro, T. Niioka, "An experimental study of droplet ignition characteristics near the ignitable limit", *Combustion and Flame*, vol. 48, pp. 27–32, 1982.

[18] J. Whang, Y. Yukao, J. Ho, S. Wong, "Experimental study of the ignition of single droplets under forced convection", *Combustion and Flame*, vol. 110, no.3, pp. 366-376, 1997.

[19] J. J. Sangiovanni, A. S. Kesten, "Effect of droplet interaction on ignition in monodispersed droplet streams", Symposium (International) on Combustion, vol. 16, no. 1, pp. 577–592, 1977.

[20] H. Chiu, T. Liu, "Group Combustion of Liquid Droplets*", Combustion Science and Technology*, vol. 17,pp. 127-142, 1977

[21] R. Yetter and I. Glassman, *Combustion*, Elsevier, 4th edition, 2008.

[22] J. C. Lasheras, I. M. Kennedy, F. L. Dryer, "Burning of Distillate Fuel Droplets Containing Alcohol or Water: Effect of Additive Concentration", *Combustion Science and Technology*, vol. 26, no. 3, pp. 161–169, 1981.

[23] T. K. Hari, Z. Yaakob, N. N. Binitha, "Aviation biofuel from renewable resources: Routes, opportunities and challenges", *Renewable Sustainable Energy Reviews*, vol. 42, pp. 1234–1244, 2015.

[24] G. Hemighaus, T. Boval, C. Bosley, *Aviation Fuels Technical Review*, Chevron, 2005.

[25] Ø. Vessia, *Biofuels from lignocellulosic material*, NTNU Norwegian University of Science and Technology, 2005.

[26] Y. X. Liu, S. Richter, C. Naumann, M. Braun-Unkhoff, Z. Y. Tian, "Combustion study of a surrogate jet fuel", *Combustion and Flame*, vol. 202, pp. 252–261, 2019.

[27] J. Hileman, H. Wong, D. Ortiz, “The feasibility and potential environmental benefits of alternative fuels for commercial aviation”, 26th International Congress of the Aeronautical Sciences, 2008.

[28] Neste Corporation, *Neste Renewable Diesel Handbook*, Neste Corporation, 2015.

[29] Y. Gong, O. Kaario, A. Tilli, M. Larmi, "A Computational Investigation of Hydrotreated Vegetable Oil Sprays Using RANS and a Modified Version of the RNG k-ε Model in OpenFOAM", SAE Technical Paper, 2010.

[30] ASTM D 1655, *Standard Specification for Aviation Turbine Fuels*, American Society for Testing and Materials, 2015.

[31] Defence Standard 91-91, *Turbine fuels, Aviation Kerosene Type, Jet A-1*, UK Ministry of Defence, 2015.

[32] U.S Department of Energies, “Alternative Aviation Fuels: Overview of challenges, Opportunities, and Next Steps”, 2016.

[33] ASTM D 7566, *Standard Specification for Aviation Turbine Fuel Containing Synthesized Hydrocarbons*, American Society for Testing and Materials, 2016.

[34] G. Simões, “Single particle ignition of pulverized solid biomass fuels : experiments and modeling”, Master thesis, Universidade Técnica de Lisboa, Instituto Superior Técnico, 2016.

[35] A. Silva, “Experimental and Numerical Study of Physical Aspects of Fuel Processes”, PhD thesis, University of Beira Interior, 2007.

[36] S. Sauer, “Investigation of Sub-Milimetric Droplet Impingement Onto Heated Surfaces”. Master thesis, Universidade Técnica de Lisboa, Instituto Superior Técnico, 2011.

[37] G. Simões, D. Magalhães, M. Rabaçal, M. Costa, “Effect of gas temperature and oxygen concentration on single particle ignition behavior of biomass fuels”, *Procedings of the Combustion Institute*, vol. 36, no. 2, pp. 2235–2242, 2017.

[38] Y. Yuan, S. Li, G. Li, N. Wu, Q. Yao, “The transition of heterogeneous-homogeneous ignitions of dispersed coal particle streams”, *Combustion and Flame*, vol. 161, no. 9, pp. 2458–2468, 2014.

[39] X. Bai, G. Lu, T. Bennet, A. Sarroza, C. Eastwick, H. Liu, Y. Yan, “Combustion behavior profiling of single pulverized coal particles in a drop tube furnace through high-speed

imaging and image analysis", *Experiments Thermal and Fluid Science*, vol. 85, pp. 322–330, 2017.

[40] B. Pizziol, M. Costa, M. O. Panão, A. Silva, "Multiple impinging jet air-assisted atomization", *Experimental Thermal and Fluid Science*, vol. 96, pp. 303–310, 2018.

[41] N. K. Patel, S. N. Shah, *Biodiesel from Plant Oils,* Elsevier 1st edition, Food, Energy, and Water: The Chemistry Connection, 2015.

[42] B. M. Igoe, M. J. Welch, "Impact of fuel contaminants on gas turbine operation", 21st Symposium of the Industrial Application of Gas Turbines Committee, 2015.

[43] H. Aatola, M. Larmi, T. Sarjovaara, S. Mikkonen, "Hydrotreated Vegetable Oil (HVO) as a Renewable Diesel Fuel: Trade-off between NOx, Particulate Emission, and Fuel Consumption of a Heavy Duty Engine", SAE International journal of Engines, 2009.

[44] J. Shinjo, J. Xia, L. C. Ganippa, A. Megaritis, "Physics of puffing and microexplosion of emulsion fuel droplets", *Physics of Fluids*, vol. 26, no. 10, 2014.

[45] Á. Muelas, P. Remacha, A. Martínez, J. Ballester, "Combustion Behavior of Jet A Droplets and its Blends With Butanol", Proceedings of ASME Turbo Expo, 2017.

[46] D. C. K. Rao, S. Karmakar, S. K. Som, "Puffing and micro-explosion behavior in combustion of butanol/Jet A-1 and acetone-butanol-ethanol (A-B-E)/Jet A-1 fuel droplets", *Combustion Science and Technology*, vol. 189, no. 10, pp. 1796–1812, 2017.

Annex

Annex 1

Dimensionless numbers

Reynolds number

The Reynolds number shows the relation between inertial and viscous forces, where μ is the dynamic viscosity of the droplet fluid:

$$Re = \frac{\rho U D_0}{\mu} = \frac{inertia\ forces}{viscous\ forces}$$

Lewis number

The Lewis number (Le) is a dimensionless number defined as the ratio of thermal diffusivity and mass diffusivity:

$$Le = \frac{\alpha}{D} = \frac{heat\ transport}{mass\ transport}$$

Schmidt number

The Schmidt number is the ratio of the kinematic viscosity and the molecular diffusion coefficient. In practice, *Sc* represents the ratio between the momentum diffusivity and the mass diffusivity:

$$Sc = \frac{\upsilon}{D} = \frac{momemtum\ transport}{mass\ transport}$$

Combustion group number

The droplet combustion group number (G) represents the ratio of gas-phase transport time to the vaporization time.

$$G = 3\left(1 + 0.276 Re^{\frac{1}{2}} Sc^{\frac{1}{2}} LeN^{\frac{2}{3}}\right)\frac{R}{S}$$